

This is my second review of this manuscript. The authors have addressed some of the concerns I had in my previous review. Re-organization of some sections has been helpful for clarity. Inclusion of the QA4ECV data is commendable. However, the authors have not addressed many of my earlier comments. Therefore, I would not recommend accepting the manuscript in the current form.

Major concerns:

1) Data/results discussed in this manuscript are based on biased slant column data and inconsistent inputs as I have discussed in detail in my previous review. Instead of revisiting the work, the authors chose to modify the version number and suggested that they will not release the data. This may be a conflict to AMT's data policy. Moreover, I could not locate how each of the comments is addressed in the revised manuscript.

As we have replied to the previous review (general comment 1), the bias in DOMINO v2 SCD should have a very small effect on our VCD results. To address this issue more clearly, here we use the SCDs of QA4ECV (to replace DOMINO v2 SCD) and re-do the VCD retrieval. As shown in Fig. S1, using QA4ECV SCD instead of DOMINO v2 SCD only improves the comparison with MAX-DOAS VCD data slightly – for example, the underestimate is reduced from 3.7% to 0.2%. Other statistics (intercept, slope, and R^2) are very similar. This test justifies our previous reasoning. We have added in the revised Appendix A (Line 623-624) that “Our test suggests that using the QA4ECV SCD data instead of DOMINO SCD data would reduce the underestimate against MAX-DOAS VCD data from 3.7% to 0.2%, a relative minor improvement.”

The main purpose of this paper is to present the substantial effect of aerosol vertical profile correction on the NO_2 retrieval. As we continuously improve the NO_2 product, we have added updates for other retrieval aspects as well. We have decided to name the intermediate product shown in this paper as v1.1, because it does not include all updates we have so far. To comply with the AMT requirement, we will provide the reader v1.1 data for the time period studied in this paper (i.e., 2012). However, for a general user of our product, we will recommend to use POMINO v2 that is available since October 2004.

We will provide a Microsoft WORD document with changes tracked.

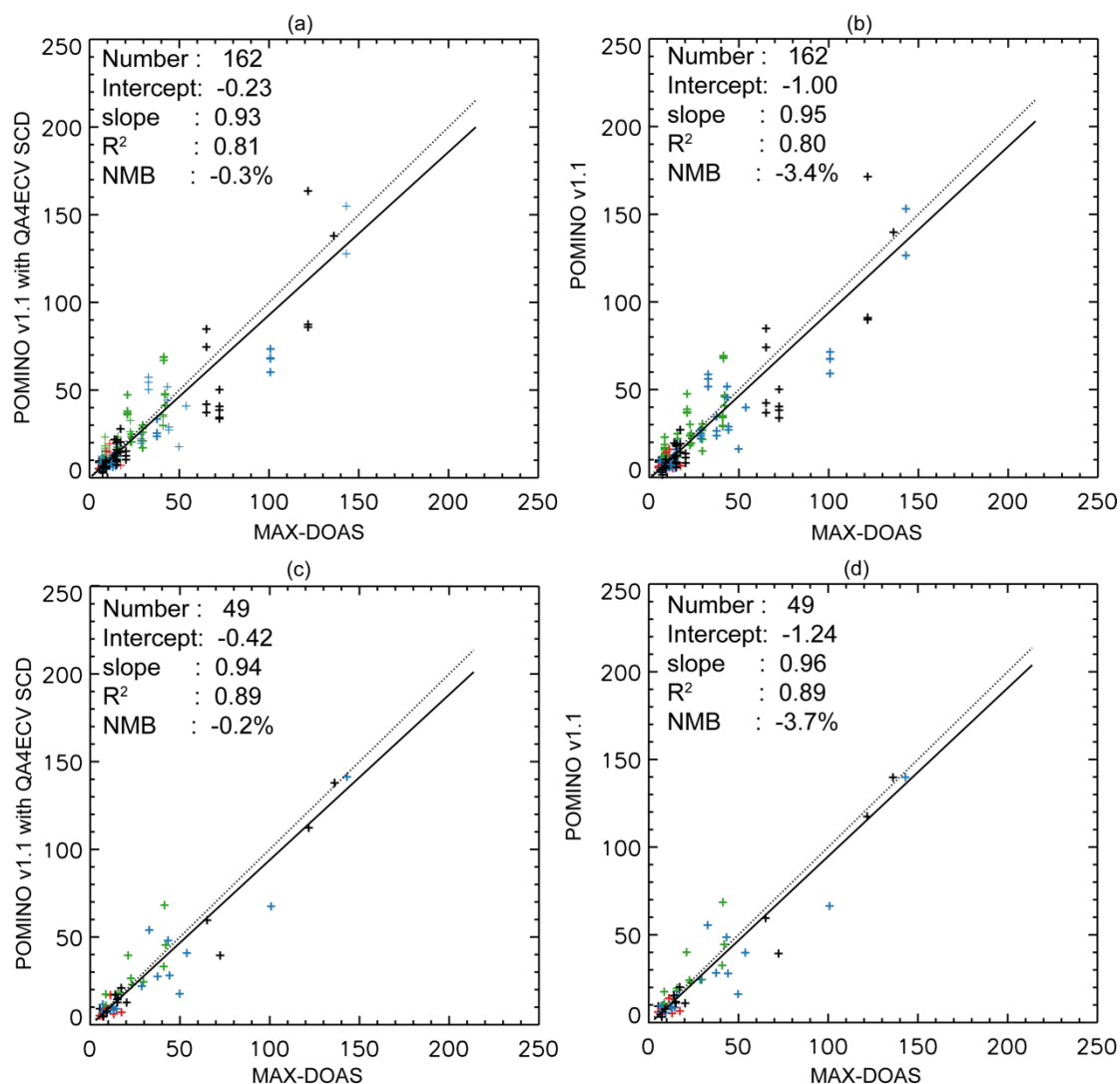


Figure S1. (a-b) Scatter plot for NO₂ VCD (10^{15} molec. cm^{-2}) between MAX-DOAS and POMINO v1.1 data with (a) QA4ECV or (b) DOMINO SCD. Each “+” corresponds to an OMI pixel, as several pixels may be available in a day. (c-d) Similar to (a-b) but after averaging over all OMI pixels in the same day, such that each “+” represents a day.

2) Their explanation for the limited number of MAX-DOAS data is well taken. But, they could still use various statistical methods and maybe other data sources to assess the improvements. Small increase in correlation alone, which may not be statistically significant, cannot be a measure of retrieval improvements (main message of this manuscript). One can raise many questions for results presented in Tables 2 and 3: What explains more than 20% difference between POMINO v1.1 and POMINO?, how is the 30% high bias of v1.1 versus MAX-DOAS an improvement?, what explains a factor of 2 difference in slope between DOMINO and QA4ECV if it is not related to slant column?, why is the comparison so poor for the improved QA4ECV OMI product?, are MAX-DOAS data accurate/reliable?, etc. From Figure 9, the relationship between DOMINO and MAX-DOAS looks much tighter as compared to POMINO and MAX-

DOAS (except for few data points) and POMINO does not show an improvement if MAX-DOAS is the ground truth.

The only difference between POMINO v1.1 and POMINO comes from the different shapes of aerosol vertical profile. Our manuscript, together with several previous studies cited in our manuscript, has clearly shown a systematic error in GEOS-Chem simulated vertical profile. Correcting for this error means an improvement of in the retrieval algorithm from POMINO to POMINO v1.1, regardless of how many MAX-DOAS (or other independent) data are available to demonstrate the algorithm improvement.

In general, the higher NO₂ VCD values in POMINO v1.1 than POMINO are because of the increased shielding effect of aerosols, which leads to smaller NO₂ AMFs. The magnitude of this increase depends on many conditions such as the fraction of clouds. In the revised manuscript, Table 2 shows a 6% increase (NMB of -9.6% versus -3.4%), Table 3 shows a 14% increase (NMB of -9.4% versus 4.4%), and Table 4 shows a 9% increase (NMB of 20.8% versus 29.4%) – these values are specific to their conditions.

Table 3 (Table 4 in our revised manuscript) basically shows that under cloud free conditions (POMINO CF = 0), the aerosol loading is much smaller than under haze days (AOD = 0.60 versus 1.13 in Table 3). In this case, POMINO v1.1, POMINO, and DOMINO v2 have similar bias (20.8%–29.4%) and R² (0.53–0.56) against MAX-DOAS NO₂ data, and the performance of QA4ECV is better. QA4ECV is essentially an ensemble of several European retrieval algorithms, all of which treat aerosols as “effective” clouds, thus its better performance (when aerosol loadings are relatively small) is not surprising. In Sect. 6, we have clarified this point that “Here, POMINO v1.1, POMINO and DONIMO v2 do not show large differences in R² (0.53–0.56) and NMB (20.8–29.4%) with respect to MAX-DOAS. QA4ECV has a higher R² (0.63) and a lower NMB (-5.8%), presumably reflecting the improvements in this (EU-) consortium approach, at least in mostly cloud-free situations. However, the R² values for POMINO and POMINO v1.1 are much smaller than the R² values in haze days, whereas the opposite changes are true for DOMINO v2 and QA4ECV. Thus, for this limited set of data, the changes from DOMINO v2 and QA4ECV to POMINO and POMINO v1.1 mainly reflect the improved aerosol treatment in hazy scenes.”

As for “what explains a factor of 2 difference in slope between DOMINO and QA4ECV if it is not related to slant column?, why is the comparison so poor for the improved QA4ECV OMI product?”, both our study and previous studies (van Geffen et al., 2015; Zara et al., 2018) show SCDs contribute insignificantly to the VCD differences. We suspect that the VCD differences come from the fact that QA4ECV is essentially an ensemble of several European retrieval algorithms. However, specific analysis of the difference between DOMINO v2 and QA4ECV is not the main topic of this study.

The reliability of MAX-DOAS data have been analyzed in many papers, including those cited in our paper (Hendrick et al., 2014; Lin et al., 2014b; Wang et al., 2017a).

In our reply to comment 3 of the previous review, we wrote that “We would definitely prefer to have a larger set of MAX-DOAS NO₂ data. Unfortunately, very few high-quality MAX-DOAS measurements are available over China. We have made efforts to get data from multiple sites to enhance the spatial representativeness.” Although we have tried very hard to get all data available, the amount of MAX-DOAS data points here do not allow to fully evaluating each satellite product. Based on this limited set of MAX-DOAS data, it is not expected that any product shows superiority in all aspects of comparison with MAX-DOAS – for example, although DOMINO v2 is a relatively older product, it may compare with (this limited set of) MAX-DOAS data better than other products under some special conditions, as pointed out by the reviewer.

Given the limited amount of available MAX-DOAS data, here we test the effect of sampling criteria (i.e., time and distance) on the comparison; the criteria chosen in the main text are described in Line 314-317, and are highlighted in bold in Tables S1 and S2. Table S1 selects OMI pixels within 25 km of MAX-DOAS sites and MAX-DOAS measurements within different hours (1 h, 1.5h, and 2 h) of OMI overpass time. For each product, the comparison results (slope, intercept, R², NMB) do not change significantly.

Table S2 selects MAX-DOAS data within 1 h of OMI overpass time and OMI pixels within various distances to MAX-DOAS sites (40 km, 35 km, 30 km, 25 km, and 20 km). For POMINO, POMINO v1.1, and POMINO v1.1 with QA4ECV SCDs, the R² value changes slightly when the distance increases from 20 km to 30 km, and starts to decline at longer distances. This reflects that as the distance increases, the satellite data tend to represent regional NO₂, in contrast to the MAX-DOAS data which are “line” measurements. Other statistics (slope, intercept, and NMB) do not change significantly with distance. Similar changes with distance are shown in DOMINO v2 and QA4ECV data.

3) The "Author's Response" does not seem to include a marked-up manuscript version. Therefore, it is not clear if the authors have sufficiently addressed the reviewers' comments and how they are addressed.

We will provide a Microsoft WORD document with changes tracked.

Minor comment:

4) It is difficult to relate the reported contents (numbers) in abstract/conclusions/discussions to tables as the tables provide results for a subset of samples but not for the entire samples. Including statistics of Figure 9 in table would be helpful.

We have added a table (Table 2) to summarize the statistics in Fig. 9, and have changed numbering of other tables accordingly.

Table S1 Evaluation of OMI products against MAX-DOAS under different temporal criteria.

	Slope			Intercept			R ²			NMB (%)		
	1h	1.5h	2h	1h	1.5h	2h	1h	1.5h	2h	1h	1.5h	2h
Hours within OMI overpass time	1h	1.5h	2h	1h	1.5h	2h	1h	1.5h	2h	1h	1.5h	2h
Number of pixels	162	175	184	162	175	184	162	175	184	162	175	184
POMINO v1.1	0.95	0.96	0.97	-1.00	-2.24	-2.42	0.80	0.77	0.76	-3.4	-5.5	-5.5
POMINO	0.78	0.80	0.80	0.96	-0.04	-0.35	0.80	0.78	0.77	-9.6	-11.3	-11.3
POMINO v1.1 (with QA4ECV SCD)	0.93	0.94	0.94	0.23	-1.57	-1.73	0.81	0.78	0.76	-0.3	-3.1	-2.5
DOMINO v2	1.06	1.10	1.10	-3.86	-5.08	-5.00	0.68	0.68	0.67	-2.1	-3.7	-2.2
QA4ECV	0.66	0.65	0.67	1.09	0.47	0.43	0.75	0.72	0.74	-22.0	-24.3	-22.7

Table S2 Evaluation of OMI products against MAX-DOAS under different spatial criteria.

Distance from MAX-DOAS site	40km	35km	30km	25km	20km	40km	35km	30km	25km	20km
Number of pixels	510	383	272	163	98	510	383	272	163	98
	slope					intercept				
POMINO v1.1	1.03	1.07	0.95	0.95	0.98	-4.87	-5.22	-1.67	-1.00	-1.57
POMINO	0.80	0.82	0.79	0.78	0.71	-0.90	-0.77	0.36	0.96	2.12
POMINO v1.1 (with QA4ECV SCD)	1.02	1.05	0.93	0.93	0.94	-3.97	-4.37	-0.70	0.23	-0.50
DOMINO v2	1.03	1.05	1.05	1.06	0.70	-3.91	-4.10	-3.49	-3.86	3.37
QA4ECV	0.64	0.64	0.65	0.66	0.65	0.15	0.45	0.86	1.09	1.34
	R ²					NMB (%)				
POMINO v1.1	0.63	0.64	0.75	0.80	0.78	-6.5	-4.9	-4.4	-3.4	-5.7
POMINO	0.69	0.71	0.75	0.80	0.80	-12.3	-11.0	-10.2	-9.6	-12.2
POMINO v1.1 (with QA4ECV SCD)	0.63	0.64	0.75	0.81	0.78	-2.1	-0.8	-0.1	-0.3	-2.4
DOMINO v2	0.60	0.63	0.66	0.68	0.63	1.5	1.2	0.6	-2.1	-5.0
QA4ECV	0.64	0.67	0.72	0.75	0.68	-22.0	-21.4	-22.0	-22.0	-23.4

1 **Improved aerosol correction for OMI tropospheric NO₂ retrieval over East Asia:**
2 **constraint from CALIOP aerosol vertical profile**

3 Mengyao Liu^{1,2}, Jintai Lin¹, K. Folkert Boersma^{2,3}, Gaia Pinardi⁴, Yang Wang⁵, Julien
4 Chimot⁶, Thomas Wagner⁵, Pinghua Xie^{7,8,9}, Henk Eskes², Michel Van Roozendaal⁴,
5 François Hendrick⁴, Pucui Wang¹⁰, Ting Wang¹⁰, Yingying Yan¹

6 1, Laboratory for Climate and Ocean-Atmosphere Studies, Department of
7 Atmospheric and Oceanic Sciences, School of Physics, Peking University, Beijing,
8 China

9 2, Royal Netherlands Meteorological Institute, De Bilt, the Netherlands

10 3, Meteorology and Air Quality department, Wageningen University, Wageningen,
11 the Netherlands

12 4, Royal Belgian Institute for Space Aeronomy (BIRA-IASB), Brussels, Belgium

13 5, Max Planck Institute for Chemistry, Mainz, Germany

14 6, Department of Geoscience and Remote Sensing (GRS), Civil Engineering and
15 Geosciences, TU Delft, the Netherlands

16 7, Anhui Institute of Optics and Fine Mechanics, Key laboratory of Environmental
17 Optics and Technology, Chinese Academy of Sciences, Hefei, China

18 8, CAS Center for Excellence in Urban Atmospheric Environment, Institute of Urban
19 Environment, Chinese Academy of Sciences, Xiamen, China

20 9, School of Environmental Science and Optoelectronic Technology, University of
21 Science and Technology of China, Hefei, China

样式定义: 标题 1: 与下段不同页

样式定义: 标题 2: 段落间距段后: 1 行, 与下段不同页

带格式的: 上标

22 10, IAP/CAS, Institute of Atmospheric Physics, Chinese Academy of Sciences,
23 Beijing, China

24 Correspondence to: Jintai Lin (linjt@pku.edu.cn); K. Folkert Boersma
25 (folkert.boersma@knmi.nl)

26 Abstract

27 Satellite retrieval of vertical column densities (VCDs) of tropospheric nitrogen
28 dioxide (NO₂) is critical for NO_x pollution and impact evaluation. For regions with
29 high aerosol loadings, the retrieval accuracy is greatly affected by whether aerosol
30 optical effects are treated implicitly (as additional “effective” clouds) or explicitly,
31 among other factors. Our previous POMINO algorithm explicitly accounts for aerosol
32 effects to improve the retrieval especially in polluted situations over China, by using
33 aerosol information from GEOS-Chem simulations with further monthly constraints
34 by MODIS/Aqua [aerosol optical depth \(AOD\)](#) data. [Here we present a major](#)
35 [algorithm update, POMINO v1.1](#), by constructing a monthly climatological data set of
36 aerosol extinction profiles, based on Level-2 CALIOP/CALIPSO data over 2007–
37 2015, to better constrain the modeled aerosol [vertical](#) profiles.

38 We find that GEOS-Chem captures the month-to-month variation of CALIOP aerosol
39 layer height but with a systematic underestimate by about 300–600 m (season and
40 location dependent), due to a too strong [negative](#) vertical gradient of extinction above
41 1 km. Correcting the model aerosol extinction profiles results in small changes in
42 retrieved cloud fraction, increases in cloud top pressure (within 2–6% in most cases),
43 and increases in tropospheric NO₂ VCD by 4–16% over China on a monthly basis in
44 2012. The improved NO₂ VCDs (in POMINO v1.1) are more consistent with
45 independent ground-based MAX-DOAS observations ($R^2 = 0.80$, NMB = -3.4% [for](#)
46 [162 pixels in 49 days](#)) than POMINO ($R^2 = 0.80$, NMB = -9.6%) [and](#) DOMINO v2 ($R^2 =$

删除的内容: t

删除的内容: AOD

删除的内容: This study is the kernel updates of our newthe retrieval algorithm, to POMINO v21.1,

删除的内容:

删除的内容: and

53 0.68, NMB = -2.1%) and QA4ECV ($R^2 = 0.75$, NMB = -22.0%) are. Especially on
54 haze days, R^2 reaches 0.76 for POMINO v1.1, much higher than that for POMINO
55 (0.68), DOMINO v2 (0.38) and QA4ECV (0.34). Furthermore, the increase in cloud
56 pressure likely reveals a more realistic vertical relationship between cloud and aerosol
57 layers, with aerosols situated above the clouds in certain months instead of always
58 below the clouds. [The POMINO v1.1 algorithm is a core step towards our next public](#)
59 [release of data product \(POMINO v2\), and it will also be applied to the recently](#)
60 [launched S5P-TropOMI sensor.](#)

61 1. Introduction

62 Air pollution is a major environmental problem in China. In particular, China has
63 become the world's largest emitting country of nitrogen oxides ($\text{NO}_x = \text{NO} + \text{NO}_2$) due
64 to its rapid economic growth, heavy industries, coal-dominated energy sources, and
65 relatively weak emission control (Cui et al., 2016; Lin et al., 2014a; Stavrou et al.,
66 2016; Zhang et al., 2009). Tropospheric vertical column densities (VCDs) of nitrogen
67 dioxide (NO_2) retrieved from the Ozone Monitoring Instrument (OMI) onboard the
68 Earth Observing System (EOS) Aura satellite have been widely used to monitor and
69 analyze NO_x pollution over China because of its high spatiotemporal coverage (e.g.
70 (Lin et al., 2010; Miyazaki and Eskes, 2013; Verstraeten et al., 2015; Zhao and Wang,
71 2009). However, NO_2 retrieved from OMI and other space-borne instruments are
72 subject to errors in the conversion process from radiance to VCD, particularly with
73 respect to the calculation of tropospheric air mass factor (AMF) that is used to convert
74 tropospheric slant column density to VCD (e.g. Boersma et al., 2011; Bucsela et al.,
75 2013; Lin et al., 2015; Lorente et al., 2017).

76 Most current-generation NO_2 algorithms do not explicitly account for the effects of
77 aerosols on NO_2 AMFs and on prerequisite cloud parameter retrievals. These
78 retrievals often adopt an implicit approach wherein cloud algorithms retrieve

带格式的: 上标

删除的内容: 82

删除的内容: 7

删除的内容:

删除的内容: and

删除的内容: This

删除的内容: improvement in ourOur POMINO v1.1 algorithm

删除的内容: ↵

87 “effective cloud” parameters that include the optical effects of aerosols. This implicit
88 method is based on aerosols exerting an effect on the top-of-atmosphere radiance
89 level, whereas the assumed cloud model does not account for the presence of aerosols
90 in the atmosphere (Stammes et al., 2008; Veeffkind et al., 2016; Wang et al., 2008b;
91 Wang and Stammes, 2014). In the absence of clouds, an aerosol optical thickness of 1
92 is then interpreted as an effective cloud fraction of ± 0.10 , and the value also depends
93 on the aerosol properties (scattering or absorbing), true surface albedo and geometry
94 angles (Chimot et al., 2016) with an effective cloud pressure closely related to the
95 aerosol layer, at least for aerosols of predominantly scattering nature (e.g. Boersma et
96 al., 2004, 2011, Castellanos et al., 2014, 2015). However, in polluted situations with
97 high aerosol loadings and more absorbing aerosol types, which often occur over
98 China and many other developing regions, the implicit method can result in
99 considerable biases (Castellanos et al., 2014, 2015; Chimot et al., 2016; Kanaya et al.,
100 2014; Lin et al., 2014b).

101 Lin et al. (2014b, 2015) established the POMINO NO₂ algorithm, which builds on the
102 DOMINO v2 algorithm (for OMI NO₂ slant columns and stratospheric correction),
103 but improves upon it through a more sophisticated AMF calculation over China. In
104 POMINO, the effects of aerosols on cloud retrievals and NO₂ AMFs are explicitly
105 accounted for. In particular, daily information on aerosol optical properties such as
106 aerosol optical depth (AOD), single scattering albedo (SSA), phase function and
107 vertical extinction profiles are taken from nested Asian GEOS-Chem v9-02
108 simulations. The modeled AOD at 550 nm is further constrained by MODIS/Aqua
109 monthly AOD, with the correction applied to other wavelengths based on modeled
110 aerosol refractive indices (Lin et al., 2014b). However, the POMINO algorithm does
111 not include an observation-based constraint on the vertical profile of aerosols, whose
112 altitude relative to NO₂ has strong and complex influences on NO₂ retrieval
113 (Castellanos et al., 2015; Leitão et al., 2010; Lin et al., 2014b). This study improves

114 upon the POMINO algorithm by incorporating CALIOP monthly climatology of
115 aerosol vertical extinction profiles to correct for model biases.

116 The CALIOP lidar, carried on the sun-synchronous CALIPSO satellite, has been
117 acquiring global aerosol extinction profiles since June 2006 (Winker et al., 2010).
118 CALIPSO and Aura are both parts of the National Aeronautics and Space
119 Administration (NASA) A-train constellation of satellites. The overpass time of
120 CALIOP/CALIPSO is only 15 minutes later than OMI/Aura. In spite of issues with
121 the detection limit, radar ratio selection and cloud contamination that cause some
122 biases in CALIOP aerosol extinction vertical profiles (Amiridis et al., 2015; Koffi et
123 al., 2012; Winker et al., 2013), comparisons of aerosol extinction profiles between
124 ground-based lidar and CALIOP show good agreements (Kacenelenbogen et al., 2014;
125 Kim et al., 2009; Misra et al., 2012). However, CALIOP is a nadir-viewing
126 instrument that measures the atmosphere along the satellite ground-track with a
127 narrow field-of-view. This means that the daily geographical coverage of CALIOP is
128 much smaller than that of OMI. Thus previous studies often used monthly/seasonal
129 regional mean CALIOP data to study aerosol vertical distributions or to evaluate
130 model simulations (Chazette et al., 2010; Johnson et al., 2012; Koffi et al., 2012; Ma
131 and Yu, 2014; Sareen et al., 2010).

132 ~~There exist a few CALIOP Level-3 gridded datasets, such as LIVAS (Amiridis et al.~~
133 ~~2015) and NASA official Level-3 monthly dataset (Winker et al., 2013). However,~~
134 ~~LIVAS is an annual average day-night combined product, not suitable to be applied to~~
135 ~~OMI NO₂ retrievals (around early afternoon, and in need of a higher temporal~~
136 ~~resolution than annual). The horizontal resolution (2° long. × 5° lat.) of NASA~~
137 ~~official product is much coarser than OMI footprints and the GEOS-Chem model~~
138 ~~resolution.~~

删除的内容: are some mature data of

删除的内容:

删除的内容: yearly

删除的内容: but

带格式的: 下标

删除的内容: measurement is only available in the daytime, besides,
the temporal resolution (yearly) is not very suitable for daily aerosol
extinction profiles usage

删除的内容: s

147 Here we construct a custom monthly climatology of aerosol vertical extinction
148 profiles based on 9-years (2007–2015) worth of CALIOP Version 3 Level-2 532 nm
149 data. On a climatological basis, we use the CALIOP monthly data to adjust
150 GEOS-Chem profiles in each grid cell for each day of the same month in any year.
151 We then use the corrected GEOS-Chem vertical extinction profiles in the retrievals of
152 cloud parameters and NO₂. Finally, we evaluate our updated POMINO retrieval
153 (hereafter referred to as POMINO v1.1), our previous POMINO product, DOMINO
154 v2, and the newly released Quality Assurance for Essential Climate Variables product
155 (QA4ECV, see Appendix A), using ground-based MAX-DOAS NO₂ column
156 measurements at three urban/suburban sites in East China for the year of 2012 and
157 several months in 2008/2009.

删除的内容: In order to constrain daily aerosol extinction profiles simulated by GEOS-Chem. However, the major monthly/seasonal CALIOP data are too coarse in spatial resolution (i.e. NASA's official monthly Level-3 CALIOP dataset with spatial resolution 2° long. × 5° lat.) or in temporal resolution (i.e. LIVAS 5-year based 1° × 1° CALIOP dataset).
H

删除的内容: and the existing

删除的内容: and

删除的内容: retrievals

158 Section 2 describes the construction of CALIOP aerosol extinction vertical profile
159 monthly climatology, the POMINO v1.1 retrieval approach, and the MAX-DOAS
160 data. It also presents the criteria for comparing different NO₂ retrieval products and
161 for selecting coincident OMI and MAX-DOAS data. Section 3 compares our CALIOP
162 climatology with NASA's official Level-3 CALIOP dataset and GEOS-Chem
163 simulation results. Sections 4 and 5 compare POMINO v1.1 to POMINO to analyze
164 the influence of improved aerosol vertical profiles on retrievals of cloud parameters
165 and NO₂ VCDs, respectively. Section 6 evaluates POMINO, POMINO v1.1, DOMINO
166 v2 and QA4ECV NO₂ VCD products using the MAX-DOAS data. Section 7
167 concludes our study.

删除的内容:

删除的内容: and

删除的内容: new released Quality Assurance for Essential Climate Variables (QA4ECV, see detailed introduction in Appendix B)

删除的内容: s

168 2. Data and methods

169 2.1 CALIOP monthly mean extinction profile climatology

删除的内容: Constructing a

170 CALIOP is a dual-wavelength polarization lidar measuring attenuated backscatter
171 radiation at 532 and 1064 nm since June 2006. The vertical resolution of aerosol

188 extinction profiles is 30 m below 8.2 km and 60 m up to 20.2 km (Winker et al., 2013),
189 with a total of 399 sampled altitudes. The horizontal resolution of CALIOP scenes is
190 335 m along the orbital track and is given over a 5 km horizontal resolution in Level-2
191 data.

192 [As detailed in Appendix B](#), we use the daily all-sky Version 3 CALIOP Level-2
193 aerosol profile product at 532 nm from 2007 to 2015 to construct a monthly Level-3
194 climatological dataset of aerosol extinction profiles over China and nearby regions.
195 [This dataset is constructed on the GEOS-Chem model grid \(0.667° long. x 0.5° lat.\)](#)
196 [and vertical resolution \(47 layers, with 36 layers or so in the troposphere\).](#)

197 The ratio of climatological monthly CALIOP to monthly GEOS-Chem profiles
198 represents the scaling profile to adjust the daily GEOS-Chem profiles in the same
199 month (see Sect. 2.2).

200 2.2 POMINO v1.1 retrieval approach

201 The NO₂ retrieval consists of three steps. First, the total NO₂ slant columns density
202 (SCD) is retrieved using the Differential Optical Absorption Spectroscopy (DOAS)
203 technique (for the 405-465 nm spectral window in the case of OMI). The uncertainty
204 of the SCD is determined by the appropriateness of the fitting technique, the
205 instrument noise, the choice of fitting window, and the orthogonality of the absorbers'
206 cross sections (Bucsela et al., 2006; van Geffen et al., 2015; Lerot et al., 2010; Richter
207 et al., 2011; Zara et al., 2018). The NO₂ SCD in DOMINO v2 has a bias at about
208 $0.5\text{--}1.3 \times 10^{15}$ molec. cm⁻² (Belmonte Rivas et al., 2014; Dirksen et al., 2011;
209 [Marchenko et al., 2015](#); van Geffen et al., 2015; Zara et al., 2018), which can be
210 reduced by improving wavelength calibration and including O₂-O₂ and liquid water
211 absorption in the fitting model (van Geffen et al., 2015). The tropospheric SCD is
212 then obtained by subtracting the stratospheric SCD from the total SCD. The bias in

删除的内容: Here

已下移 [5]: We choose the all-sky product instead of clear-sky data, since previous studies indicate that the climatological aerosol extinction profiles are affected insignificantly by the presence of clouds (Koffi et al. 2012; Winker et al. 2013). As we use this climatological data to adjust GEOS-Chem results, choosing all-sky data improves consistency with the model simulation when doing the daily correction.

已下移 [1]: In brief, only the pixels with Cloud Aerosol Discrimination (CAD) scores between -20 and -100 with extinction Quality Control (QC) flag valued at 0, 1, 18, and 16 are selected. We further discard samples with an extinction uncertainty of 99.9 km⁻¹, which is indicative of unreliable retrieval. We only accept extinction values falling in the range from 0.0 to 1.25, according to CALIOP observation thresholds. Previous studies showed that weakly scattering edges of icy clouds are sometimes misclassified as aerosols (Winker et al. 2013). To eliminate contamination from icy clouds we exclude the aerosol layers above the cloud layer (with layer-top temperature below 0 °C) when both of them are above 4km (Winker et al. 2013).

已下移 [2]: CALIOP Level-2 data are always presented at the fixed 399 altitudes above sea level. To account for the difference in surface elevation between a CALIOP pixel and the respective model grid cell,

删除的内容: We apply a number of criteria to ensure data quality of each pixel, mainly following Winker et al. (2013) and Amiridis et al. ... [1]

带格式的: 非突出显示

删除的内容:

删除的内容: After the pixel-based screening, we aggregate the CALIOP data at the model grid (0.667° long. x 0.5° lat.) and vertical ... [2]

删除的内容:

已下移 [3]: Figure 1 shows the number of aerosol extinction profiles in each grid cell and 12 x 9 = 108 months that are used to compile the

删除的内容: ... [3]

删除的内容: As discussed above, we choose the CALIOP pixels within 1.5° of a grid cell center. We test this choice by examining the ... [3]

已下移 [4]: For each grid cell in each month, we further correct singular values in the vertical profile. In a month, if a grid cell i has

批注 [JL1]: Add Zara et al. (2018)

337 the total SCD is mostly absorbed by this stratospheric separation step, which ~~may~~ not
338 propagate into the tropospheric SCD (van Geffen et al., 2015). The last step converts
339 the tropospheric SCD to VCD by using the tropospheric AMF ($VCD = SCD / AMF$).
340 The tropospheric AMF is calculated ~~at 438 nm~~ by using look-up tables (in most
341 retrieval algorithms) or online radiative transfer modeling (in POMINO) ~~driven by~~
342 ancillary parameters, which act as the dominant source of errors in retrieved NO₂
343 VCD data over polluted areas (Boersma et al., 2007; Lin et al., 2014b, 2015; Lorente
344 et al., 2017).

删除的内容:

删除的内容: will

删除的内容: at 439 nm

345 Our POMINO algorithm focuses on the tropospheric AMF calculation over China and
346 ~~nearby~~ regions, taking the tropospheric SCD (Dirksen et al., 2011) from DOMINO v2
347 (Boersma et al., 2011). POMINO improves upon the DOMINO v2 algorithm in the
348 treatment of aerosols, surface reflectance, online radiative transfer calculations, spatial
349 resolution of NO₂, ~~temperature and pressure~~ vertical profiles, ~~and~~ consistency
350 between cloud and NO₂ retrievals (Lin et al., 2014b, 2015). In brief, we use the
351 parallelized LIDORT-driven AMFv6 package to derive both cloud parameters and
352 tropospheric NO₂ AMFs for individual OMI pixels, ~~online~~, NO₂ vertical profiles,
353 aerosol optical properties and aerosol vertical profiles are taken from the nested
354 GEOS-Chem model over Asia ($0.667^\circ \text{ long.} \times 0.5^\circ \text{ lat.}$ before May 2013 and
355 $0.3125^\circ \text{ long.} \times 0.25^\circ \text{ lat.}$ afterwards), and pressure and temperature profiles are
356 taken from the GEOS-5 and GEOS-FP assimilated meteorological fields that drive
357 GEOS-Chem simulations. Model aerosols are further adjusted by satellite data (see
358 below). We adjust the pressure profiles based on the difference in elevation between
359 the pixel center and the matching model grid cell (Zhou et al., 2010). We also account
360 for the effects of surface bidirectional reflectance distribution function (BRDF) (Lin
361 et al., 2014b; Zhou et al., 2010) by taking three kernel parameters (isotropic,
362 volumetric and geometric) from the MODIS MCD43C2 data set at 440 nm (Lucht et
363 al., 2000).

删除的内容: nearby

删除的内容: , improved surface elevation

删除的内容: and other aspects

删除的内容:

删除的内容: without use of look-up tables

删除的内容:

删除的内容:

374 As a prerequisite to the POMINO NO₂ retrieval, clouds are retrieved through the
375 O₂-O₂ algorithm (Acarreta et al., 2004; Stammes et al., 2008) with O₂-O₂ SCDs from
376 OMCLDO2, and with pressure, temperature, surface reflectance, aerosols and other
377 ancillary information consistent with the NO₂ retrieval. Note that the treatment of
378 cloud scattering (as “effective” Lambertian reflector, as in other NO₂ algorithms) is
379 different from the treatment of aerosol scattering/absorption (vertically resolved based
380 on the Mie scheme).

381 POMINO uses the temporally and spatially varying aerosol information, including
382 AOD, single scattering albedo (SSA), phase function and vertical profiles from
383 GEOS-Chem simulations. POMINO v1.1 (this work) further uses CALIOP data to
384 constrain the shape of aerosol vertical extinction profile. We run the model at a
385 resolution of 0.3125° long. × 0.25° lat. before May 2013 and 0.667° long. ×
386 0.5° lat. afterwards, as determined by the resolution of the driving meteorological
387 fields. We then regrid the finer resolution model results to 0.667° long. × 0.5° lat., to
388 be consistent with the CALIOP data grid. We then sample the model data at times and
389 locations with valid CALIOP data at 532 nm to establish the model monthly
390 climatology.

391 For any month in a grid cell, we divide the CALIOP monthly climatology of aerosol
392 extinction profile shape by model climatological profile shape to obtain a unitless
393 scaling profile (Eq. 1), and apply this scaling profile to all days of that month in all
394 years (Eq. 2). Such a climatological adjustment is based on the assumption that
395 systematic model limitations are month-dependent and persist over the years and days
396 (e.g., a too strong vertical gradient, see Sect. 3.3). Although this monthly adjustment
397 means discontinuity on the day-to-day basis (e.g., from the last day of a month to the
398 first day of the next month), such discontinuity does not significantly affect the NO₂
399 retrieval, based on our sensitivity test.

删除的内容: the

删除的内容: al is done

带格式的: 下标

删除的内容: It should be noticed

删除的内容: s

带格式的: 下标

删除的内容: scattering by clouds and

删除的内容: s in tropospheric AMF calculation are different. The cloud are treated as lambert reflector while Mie scattering scheme is used for aerosols in RTM calculations

删除的内容:

删除的内容:

删除的内容:

删除的内容: 2

删除的内容: 3

带格式的: 下标

删除的内容: significantly

414 In Eqs. 1 and 2, E^C represents the CALIOP climatological aerosol extinction
 415 coefficient, E^G the GEOS-Chem extinction, E^{Gr} the post-scaling model extinction,
 416 and R the scaling profile. The subscript i denotes a grid cell, k a vertical layer, d a day,
 417 m a month, and y a year. Note that in Eq. 1, the extinction coefficient at each layer is
 418 normalized relative to the maximum value of that profile. This procedure ensures that
 419 the scaling is based on the relative shape of the extinction profile and is thus
 420 independent of the accuracies of CALIOP and GEOS-Chem AOD. We keep the
 421 absolute AOD value of GEOS-Chem unchanged in this step.

删除的内容: Actually, the correction to model simulated aerosol extinction profiles are main restricted by observation. CALIOP observation are only one highly spatialtemporal coverage data we can find.

删除的内容: 2

删除的内容: 3

删除的内容:

删除的内容: 2

$$422 R_{i,k,m} = \frac{E_{i,k,m}^C / \max(E_{i,k,m}^C)}{E_{i,k,m}^G / \max(E_{i,k,m}^G)} \quad (1)$$

删除的内容: 2

$$423 E_{i,k,d,m,y}^{Gr} = E_{i,k,d,m,y}^G \times R_{i,k,m} \quad (2)$$

删除的内容: 3

424 In POMINO, the GEOS-Chem AOD are further constrained by a MODIS/Aqua
 425 Collection 5.1 monthly AOD dataset compiled on the model grid (Lin et al., 2014b,
 426 2015). POMINO v1.1 uses the Collection 5.1 AOD data before May 2013 and
 427 Collection 6 data afterwards. For adjustment, model AOD are projected to a
 428 $0.667^\circ \text{ long.} \times 0.5^\circ \text{ lat.}$ grid and then sampled at times and locations with valid
 429 MODIS data (Lin et al., 2015). As shown in Eq. 3, τ^M denotes MODIS AOD, τ^G
 430 GEOS-Chem AOD, and τ^{Mr} post-adjustment model AOD. The subscript i denotes
 431 a grid cell, d a day, m a month, and y a year. This AOD adjustment ensures that in any
 432 month, monthly mean GEOS-Chem AOD is the same as MODIS AOD while the
 433 modeled day-to-day variability is kept.

删除的内容:

删除的内容: 4

$$434 \tau_{i,d,m,y}^{Gr} = \frac{\tau_{i,m,y}^M}{\tau_{i,m,y}^G} \times \tau_{i,d,m,y}^G \quad (3)$$

删除的内容: 4

435 Equations 4-5 show the complex effects of aerosols in calculating the AMF for any
 436 pixel. The AMF is the linear sum of tropospheric layer contributions to the slant

删除的内容: 5

删除的内容: 6

452 column weighted by the vertical subcolumns (Eq. 4). The box AMF, amf_k , describes
 453 the sensitivity of NO₂ SCD to layer k , and $x_{a,k}$ represent the subcolumn of layer k
 454 from a priori NO₂ profile. The l represent the first integrated layer, which is the layer
 455 above the ground for clear sky, or the layer above cloud top for cloudy sky. The t
 456 represent the tropopause layer. POMINO assumes the independent pixel
 457 approximation (IPA) (Martin *et al.*, 2002; Boersma *et al.*, 2002). This means that the
 458 calculated AMF for any pixel consists of a fully cloudy-sky portion (AMF_{ctr}) and a
 459 fully clear-sky portion (AMF_{cld}), with weights based on the cloud radiance fraction
 460 ($CRF = (1 - CF) \cdot A_{clr} + CF \cdot A_{cld}$, A_{clr} , A_{cld} are radiance from the clear-sky part
 461 and cloudy part of the pixel, respectively.) (Eq. 5). AMF_{cld} is affected by
 462 above-cloud aerosols, and AMF_{ctr} is affected by aerosols in the *entire* column. Also,
 463 aerosols affect the retrieval of CRF. Thus, the improvement of aerosol vertical profile
 464 in POMINO v1.1 affects all the three quantities in Eq. 5 and thus leads to complex
 465 impacts on retrieved NO₂ VCD.

删除的内容: 5

删除的内容: CRF

删除的内容: 6

删除的内容: whole

删除的内容: 6

$$466 \quad AMF = \frac{\sum_l^t amf_k x_{a,k}}{\sum_l^t x_{a,k}} \quad (4)$$

删除的内容: 5

$$467 \quad AMF = AMF_{cld} \cdot CRF + AMF_{ctr} \cdot (1 - CRF) \quad (5)$$

删除的内容: 6

468 2.3 OMI pixel selection to evaluate POMINO v1.1, POMINO, DOMINO v2 and 469 QA4ECV

删除的内容: and

470 We exclude OMI pixels affected by row anomaly (Schenkeveld *et al.*, 2017) or with
 471 high albedo caused by icy/snowy ground. To screen out cloudy scenes, we choose
 472 pixels with CRF below 50% (effective cloud fraction is typically below 20%) in
 473 POMINO.

474 The selection of CRF threshold influences the validity of pixels. The “effective” CRF
 475 in DOMINO implicitly includes the influence of aerosols. In POMINO, the aerosol

484 contribution is separated from that of the clouds, resulting in a lower CRF than for
485 DOMINO. The CRF differs insignificantly between POMINO and POMINO v1.1,
486 because the same AOD and other non-aerosol ancillary parameters are used in the
487 retrieval process. Using the CRF from POMINO instead of DOMINO or QA4ECV
488 for cloud screening means that the number of “valid” pixels in DOMINO increases by
489 about 25%, particularly because much more pixels with high pollutant (aerosol and
490 NO₂) loadings are now included. This potentially reduces the sampling bias (Lin et al.,
491 2014b, 2015), and the ensemble of pixels now includes scenes with high “aerosol
492 radiative fractions”. Further research is needed to fully understand how much these
493 high-aerosol scenes may be subject to the same screening issues as the cloudy scenes.
494 Nevertheless, the limited evidence here and in Lin et al. (2014b, 2015) suggests that
495 including these high-aerosol scenes does not affect the accuracy of NO₂ retrieval.

496 2.4 MAX-DOAS data

497 We use MAX-DOAS measurements at three suburban or urban sites in East China,
498 including one urban site at the Institute of Atmospheric Physics (IAP) in Beijing
499 (116.38° E, 39.38° N), one suburban site in Xianghe County (116.96° E, 39.75° N)
500 to the south of Beijing, and one urban site in the Wuxi City (120.31° E, 31.57° N) in
501 the Yangzi River delta (YRD). Figure 1 shows the locations of these sites overlaid
502 with POMINO v1.1 NO₂ VCDs in August 2012. Table 1 summarizes the information
503 of MAX-DOAS measurements.

504 The instruments in IAP and in Xianghe were designed at BIRA-IASB (Clémer et al.,
505 2010). Such an instrument is a dual-channel system composed of two thermally
506 regulated grating spectrometers, covering the ultraviolet (300–390 nm) and visible
507 (400–720 nm) wavelengths. It measures scattered sunlight every 15 minutes at nine
508 elevation angles: 2° , 4° , 6° , 8° , 10° , 12° , 15° , 30° , and 90° . The
509 telescope of the instrument is pointed to the north. The data are analyzed following

删除的内容: but

删除的内容: the drawback is that

删除的内容: ing

删除的内容: although

删除的内容: 2

删除的内容: 2

516 Hendrick et al. (2014). The Xianghe suburban site is influenced by pollution from the
517 surrounding major cities like Beijing and Tianjin. At Xianghe, MAX-DOAS data are
518 data are continuously available since early 2011, and data in 2012 are used here for
519 comparison with OMI products. At IAP, MAX-DOAS data are available in 2008 and
520 2009 (Table 1), thus for comparison purposes we process OMI products to match the
521 MAX-DOAS times.

删除的内容: 2

522 Located on the roof of an 11-story building, the instrument at Wuxi was developed by
523 Anhui Institute of Optics and Fine Mechanics (AIOFM) (Wang et al., 2015, 2017a).
524 Its telescope is pointed to the north and records at five elevation angles (5° , 10° ,
525 20° , 30° and 90°). Wuxi is a typical urban site affected by heavy NO_x and
526 aerosol pollution. The measurements used here are analyzed in Wang et al. (2017a).
527 Data are available in 2012 for comparison with OMI products.

528 When comparing the four OMI products against MAX-DOAS observations, temporal
529 and spatial inconsistency in sampling is inevitable. The spatial inconsistency, together
530 with the substantial horizontal inhomogeneity in NO_2 , might be more important than
531 the influence of temporal inconsistency (Wang et al., 2017b). The influence of the
532 horizontal inhomogeneity was suggested to be about 10–30% for MAX-DOAS
533 measurements in Beijing (Lin et al., 2014b; Ma et al., 2013) and 10–15% for less
534 polluted locations like Tai'an, Mangshan and Rudong (Irie et al., 2012). Following
535 previous studies (Lin et al., 2014b; Wang et al., 2015, 2017b), we average
536 MAX-DOAS data within 2 h of the OMI overpass time, and we select OMI pixels
537 within 25 km of a MAX-DOAS site whose viewing zenith angle is below 30° . To
538 exclude local pollution events near the MAX-DOAS site (such as the abrupt increase
539 of NO_2 caused by the pass of consequent vehicles during a very short period), the
540 standard deviation of MAX-DOAS data within 2 h should not exceed 20% of their

删除的内容: three

543 mean value (Lin et al., 2014b). We elect not to spatially average the OMI pixels
544 because they can, to some degree, reflect the spatial variability in NO₂ and aerosols.

删除的内容: to some degree

545 We further exclude MAX-DOAS data in cloudy conditions, as clouds can cause large
546 uncertainties in MAX-DOAS and OMI data. To find the actual cloudy days, we use
547 MODIS/Aqua cloud fraction data, MODIS/Aqua Level-3 corrected reflectance (true
548 color) data at the 1° x 1° resolution, and current weather data observed from the
549 nearest ground meteorological station (indicated by the black triangles in Fig. 1b).

删除的内容: 2

550 Since there is only one meteorological station available near the Beijing area, it is
551 used for both IAP and Xianghe MAX-DOAS sites. We first use MODIS/Aqua
552 corrected reflectance (true color) to distinguish clouds from haze. For cloudy days
553 determined by the reflectance checking, we examine both the MODIS/Aqua cloud
554 fraction data and the meteorological station cloud records, considering that
555 MODIS/Aqua cloud fraction data may be missing or have a too coarse horizontal
556 resolution to accurately interpret the cloud conditions at the MAX-DOAS site. We
557 exclude MAX-DOAS NO₂ data if the MODIS/Aqua cloud fraction is larger than 60%
558 and the meteorological station reports a “BROKEN” (cloud fraction ranges from 5/8
559 to 7/8) or “OVERCAST” (full cloud cover) sky. For the three MAX-DOAS sites
560 together, this leads to 49 days with valid data out of 64 days with pre-screening data.

561 We note here that using cloud fraction data from MODIS/Aqua or MAX-DOAS (for
562 Xianghe only, see Gielen et al., 2014) alone to screen cloudy scenes may not be
563 appropriate on heavy-haze days. For example, on 8th January, 2012, MODIS/Aqua
564 cloud fraction is about 70–80% over the North China Plain and MAX-DOAS at
565 Xianghe suggests the presence of “thick clouds”. However, both the meteorological
566 station and MODIS/Aqua corrected reflectance (true color) product suggest that the
567 North China Plain was covered by a thick layer of haze. Consequently, this day was
568 excluded from the analysis.

571 **3. Monthly climatology of aerosol extinction profiles from CALIOP and**
572 **GEOS-Chem**

573 *3.1 CALIOP monthly climatology*

574 The [aerosol layer height \(ALH\)](#) is a good indicator to what extent aerosols are mixed
575 vertically ([Castellanos et al., 2015](#)). [As defined in Eq. A1 in Appendix B, the ALH is](#)
576 [the average height of aerosols weighted by vertically resolved aerosol extinction.](#)

577 Figure [2a](#) shows the spatial distribution of our CALIOP ALH climatology in each
578 season. At most places, the ALH reaches a maximum in spring or summer and a
579 minimum in fall or winter. The lowest ALH in fall and winter can be attributed to
580 heavy near-surface pollution and weak vertical transport. The high values in summer
581 are related to strong convective activities. Over the north, the high values in spring are
582 partly associated with Asian dust events, due to high surface winds and dry soil in this
583 season ([Huang et al., 2010](#); [Proestakis et al., 2017](#); [Wang et al., 2010](#)), which also
584 affects the oceanic regions via atmospheric transport. The springtime high ALH over
585 the south may be related to the transport of carbonaceous aerosols from Southeast
586 Asian biomass burning ([Jethva et al., 2016](#)). Averaged over the domain, the seasonal
587 mean ALHs are 1.48 km, 1.43 km, 1.27km, 1.18 km in spring, summer, fall and
588 winter.

589 Figure [3a,b](#) further shows the climatological monthly variations of ALH averaged
590 over Northern East China (the anthropogenic source region shown in orange in Fig. [1a](#))
591 and Northwest China (the dust source region shown in yellow in Fig. [1a](#)). The two
592 regions exhibit distinctive temporal variations. Over Northern East China, the ALH
593 reaches a maximum in April (~1.53 km) and a minimum in December (~1.14 km).
594 Over Northwest China, the ALH peaks in August (~1.59km) because of strongest
595 convection ([Zhu et al., 2013](#)), although the springtime ALH is also high.

删除的内容: 3

删除的内容: 4

删除的内容: 2

删除的内容: 2

600 Figure 4a shows the climatological seasonal regional average vertical profiles of
601 aerosol extinction over Northern East China. Here, the aerosol extinction increases
602 from the ground level to a peak at about 300–600 m (season dependent), above which
603 it decreases gradually. The height of peak extinction is lowest in winter, consistent
604 with a stagnant atmosphere, thin mixing layer, and increased emissions (from
605 residential and industrial sectors). The large error bars (horizontal lines in different
606 layers, standing for 1 standard deviation) indicate strong spatiotemporal variability of
607 aerosol extinction.

删除的内容: 5

608 Over Northwest China (Fig. 5a), the column total aerosol extinction is much smaller
609 than that over Northern East China (Fig. 4a), due to lower anthropogenic sources and
610 dominant natural dust emissions. Vertically, the decline of extinction from the
611 peak-extinction height to 2 km is also much more gradual than the decline over
612 Northern East China, indicating stronger lifting of surface emitted aerosols. In winter,
613 the column total aerosol extinction is close to the high value in dusty spring, whereas
614 the vertical gradient of extinction is strongest among the seasons. This reflects the
615 high anthropogenic emissions in parts of Northwest China, which have been rapidly
616 increasing in the 2000s due to relatively weak emission control supplemented by
617 growing activities of relocation of polluted industries from the eastern coastal regions
618 (Cui et al., 2016; Zhao et al., 2015).

删除的内容: 6

删除的内容: 5

删除的内容: 3

删除的内容: C

删除的内容: 3.2 Comparison to NASA CALIOP monthly climatology
We compare our gridded climatological profiles to NASA CALIOP Version 3 Level-3 all-sky monthly profiles at 532 nm (Winker et al. 2013). The NASA Level-3 data has a horizontal resolution of $2^\circ \text{ lat.} \times 5^\circ \text{ lon.}$ and a vertical resolution of 60 m (from -0.5 to 12 km above sea level). We combine NASA monthly data over 2007–2015 to construct a monthly climatology for comparison with our own compilation. We only choose aerosol extinction data in the troposphere with error less than 0.15 (the valid range given in the CALIOP dataset). If the number of valid monthly profiles in a grid cell is less than five (i.e., for the same month in five out of the nine years), then we exclude data in that grid cell; see the dark gray grid cells in Fig. 23c. ↵

Several methodological differences exist between generating our and NASA CALIOP datasets. First, the two datasets have different horizontal resolutions. Also, we sample all valid CALIOP pixels within 1.5° of a grid cell center, whereas the NASA dataset samples all valid pixels within a grid cell. Besides, our CALIOP dataset involves several steps of horizontal interpolation, for purposes of subsequent cloud and NO_2 retrievals, which is not done in the NASA dataset. In addition, we match CALIOP data vertically to the GEOS-Chem vertical resolution, whereas the NASA dataset maintains the original resolution. ↵

... [4]

删除的内容: 3

619 Overall, the spatial and seasonal variations of CALIOP aerosol vertical profiles are
620 consistent with changes in meteorological conditions, anthropogenic sources, and
621 natural emissions. The data will be used to evaluate and adjust GEOS-Chem
622 simulation results in Sect. 3.2. [A comparison of our CALIOP dataset with NASA's
623 official Level-3 data is presented in Appendix C.](#)

624 [3.2 Evaluation of GEOS-Chem aerosol extinction profiles](#)

692 Figure 2b shows the spatial distribution of seasonal ALHs simulated by GEOS-Chem.
693 The model captures the spatial and seasonal variations of CALIOP ALH (Fig. 2a) to
694 some degree, with an underestimate by about 0.3 km on average. The spatial
695 correlation between CALIOP (Fig. 2a) and GEOS-Chem (Fig. 2b) ALH is 0.37 in
696 spring, 0.57 in summer, 0.40 in fall, and 0.44 in winter. The spatiotemporal
697 consistency and underestimate is also clear from the regional mean monthly ALH data
698 in Fig. 3 – the temporal correlation between GEOS-Chem and CALIOP ALH is 0.90
699 in Northern East China and 0.97 in Northwest China.

700 Figures 4a and 5a show the GEOS-Chem simulated 2007–2015 monthly
701 climatological vertical profiles of aerosol extinction coefficient over Northern East
702 China and Northwest China, respectively. Over Northern East China (Fig. 4a), the
703 model (red line) captures the vertical distribution of CALIOP extinction (black line)
704 below the height of 1 km, despite a slight underestimate in the magnitude of
705 extinction and an overestimate in the peak-extinction height. From 1 to 5 km above
706 the ground, the model substantially overestimates the rate of decline in extinction
707 coefficient with increasing altitude. Across the seasons, GEOS-Chem underestimates
708 the magnitude of aerosol extinction by up to 37% (depending on the height). Over
709 Northwest China (Fig. 5a), GEOS-Chem has an underestimate in all seasons, with the
710 largest bias by about 80% in winter likely due to underestimated water-soluble
711 aerosols and dust emissions (Li et al., 2016; Wang et al., 2008a).

712 Since the POMINO v1.1 algorithm uses MODIS AOD to adjust model AOD, it only
713 uses the CALIOP aerosol extinction profile shape to adjust the modeled shape (Eqs. 1
714 and 2). Figures 4b and 4c show the vertical shapes of aerosol extinction, averaged
715 across all profiles in each season over Northern East China and Northwest China,
716 respectively. Over Northern East China (Fig. 4b), GEOS-Chem underestimates the
717 CALIOP values above 1 km by 52–71%. This underestimate leads to a lower ALH,

删除的内容: 3

删除的内容: 3

删除的内容: 3

删除的内容: 3

删除的内容: 4

删除的内容: 5

删除的内容: 6

删除的内容: 5

删除的内容: 6

删除的内容: 2

删除的内容: 3

删除的内容: 5

删除的内容: 6

删除的内容: 5

732 consistent with the finding by van Donkelaar et al. (2013) and Lin et al. (2014b). Over
733 Northwest China (Fig. 5b), the model also underestimates the CALIOP values above
734 1 km by 50–62%. These results imply the importance of correcting the modeled
735 aerosol vertical shape prior to cloud and NO₂ retrievals.

删除的内容: 6

736 4. Effects of aerosol vertical profile improvement on cloud retrieval in 2012

737 Figure 6a, b shows the monthly average ALH and cloud top height (CTH,
738 corresponding to cloud pressure, CP) over Northern East China and Northwest China
739 in 2012. In order to discuss the CTH, only cloudy days are analyzed here, by
740 excluding days with zero cloud fraction (CF = 0, clear-sky cases) in POMINO.
741 Although “clear sky” is used sometimes in the literature to represent low cloud
742 coverage (e.g., CF < 0.2 or CRF < 0.5, Boersma et al., 2011; Chimot et al., 2016),
743 here it strictly means CF = 0 while “cloudy sky” means CF > 0. About 62.7% of days
744 contain non-zero fractions of clouds over Northern East China, and the number is 59.1%
745 for Northwest China. The CF changes from POMINO to POMINO v1.1 (i.e., after
746 aerosol vertical profile adjustment) are negligible (within ±0.5%, not shown) due to
747 the same values of AOD and SSA used in both products. This is because overall CF is
748 mostly driven by the continuum reflectance at 475 nm (mainly determined by AOD
749 and surface reflectance, which remain unchanged), which is independent of aerosol
750 profile but CTH is driven by the O₂-O₂ SCD, which is itself impacted by ALH.

删除的内容: 7

751 Figure 6a, b shows that over the two regions, the CTH varies notably from one month
752 to another, whereas the ALH is much more stable across the months. Over Northern
753 East China, the ALH increases by 0.52 km from POMINO (orange dashed line) to
754 POMINO v1.1 (orange solid line) due to the CALIOP-based monthly climatological
755 adjustment. The increase in ALH means a stronger “shielding” effect of aerosols on
756 the O₂-O₂ absorbing dimer, which, in turn, results in a reduced CTH by 0.69 km on
757 average. For POMINO over Northern East China (Fig. 6a), the retrieved clouds

删除的内容: 7

删除的内容: 7

762 usually extend above the aerosol layer, i.e., the CTH (grey dashed line) is much larger
763 than the ALH (orange dashed line). Using the CALIOP climatology in POMINO v1.1
764 results in the ALH higher than the CTH in fall and winter. The more elevated ALH is
765 consistent with the finding of Jethva et al. (2016) that a significant amount of
766 absorbing aerosols resides above clouds over Northern East China based on 11-year
767 (2004–2015) OMI near-UV observations.

768 The CTH in Northwest China is much lower than in Northern East China (Fig. 6a
769 versus 7b). This is because the dominant type of actual clouds is (optically thin) cirrus
770 over western China (Wang et al., 2014), which is interpreted by the O₂-O₂ cloud
771 retrieval algorithm as reduced CTH (with cloud base from the ground). The reduction
772 in CTH from POMINO to POMINO v1.1 over Northwest China is also smaller than
773 the reduction over Northern East China, albeit with a similar enhancement in ALH,
774 due to lower aerosol loadings (Fig. 6c versus 6d).

775 Figure 7g,h presents the relative change in CP from POMINO to POMINO v1.1 as a
776 function of AOD (binned at an interval of 0.1) and changes in ALH from POMINO to
777 POMINO v1.1 (Δ ALH, binned every 0.2 km) across all pixels in 2012 over Northern
778 East China. Results are separated for low cloud fraction ($CF < 0.05$ in POMINO, Fig.
779 7g) and modest cloud fraction ($0.2 < CF < 0.3$, Fig. 7h). The median of the CP
780 changes for pixels within each AOD and Δ ALH bin is shown. Figure 7e,f presents the
781 corresponding numbers of occurrence under the two cloud conditions.

782 Figure 7 shows that over Northern East China, the increase in ALH is typically within
783 0.6 km for the case of $CF < 0.05$ (Fig. 7e), and the corresponding increase in CP is
784 within 6% (Fig. 7g). In this case, the average CTH (2.95 km in POMINO versus 1.58
785 km in POMINO v1.1) becomes much lower than the average ALH (1.06 km in
786 POMINO versus 1.98 km in POMINO v1.1). For the case with CF between 0.2 and
787 0.3, the increase in ALH is within 1.2 km for most scenes (Fig. 7f), which leads to a

删除的内容: 7

删除的内容: 7

删除的内容: 7

删除的内容: 8

799 CP change of 2% (Fig. 7h), much smaller than the CP change for $CF < 0.05$ (Fig. 7g).
800 This is partly because the larger the CF is, the smaller a change in CF is required to
801 compensate for the ΔALH in the O_2-O_2 cloud retrieval algorithm. Furthermore, with
802 $0.2 < CF < 0.3$, the mean value of CTH is much higher than ALH in both POMINO
803 (2.76 km for CTH versus 1.13km for ALH) and POMINO v1.1 (2.60km for CTH
804 versus 2.09 km for ALH), thus a large portion of clouds are above aerosols so that the
805 change in CP is less sensitive to ΔALH . We find that the summertime data contribute
806 the highest portion (36.5%) to the occurrences for $0.2 < CF < 0.3$.

807 For Northwest China (not shown), the dependence of CP changes to AOD and ΔALH
808 is similar to that for Northern East China. In particular, the CP change is within 10%
809 on average for the case of $CF < 0.05$ and 1.5% for the case of $0.2 < CF < 0.3$.

810 5. Effects of aerosol vertical profile improvement on NO_2 retrieval in 2012

811 Figure 7a presents the percentage changes in clear-sky NO_2 VCD from POMINO to
812 POMINO v1.1 as a function of binned AOD and ΔALH over Northern East China.
813 Here, clear-sky pixels are chosen based on $CF = 0$ in POMINO. In any AOD bin, an
814 increase in ΔALH leads to an enhancement in NO_2 . And for any ΔALH , the change in
815 VCD is greater (smaller) when AOD becomes larger (smaller), which indicates that
816 the NO_2 retrieval is more sensitive to ALH in high aerosol loading cases. Clearly, the
817 change in NO_2 is not a linear function of AOD and ΔALH .

818 For cloudy scenes (Fig. 7b,c, cloud data are based on POMINO), the change in NO_2
819 VCD is less sensitive to AOD and ΔALH . This is because the existence of clouds
820 limits the optical effect of aerosols on tropospheric NO_2 . Figure 6a presents the
821 nitrogen layer height (NLH, defined as the average height of model simulated NO_2
822 weighted by its volume mixing ratio in each layer) in comparison to the ALH and
823 CLH over Northern East China. The figure shows that the POMINO v1.1 CTH is

删除的内容: 8

删除的内容: 8

删除的内容: 8

删除的内容: 8

删除的内容: 7

829 higher than the NLH in all months and higher than the ALH in warm months, which
830 means a “shielding” effect on both NO₂ and aerosols.

831 Over Northwest China (not shown), the changes in clear-sky NO₂ VCD are within 9%
832 for most cases, which are much smaller than over Eastern China (within 18%). This is
833 because the NLH is much higher than the CLH and ALH (Fig. 6b) in absence of
834 surface anthropogenic emissions.

835 We convert the valid pixels into monthly mean Level-3 values datasets on a 0.25°
836 long. × 0.25° lat. grid. Figure 8a,b compares the seasonal spatial variations of NO₂
837 VCD in POMINO v1.1 and POMINO in 2012. In both products, NO₂ peaks in winter
838 due to the longest lifetime and highest anthropogenic emissions (Lin, 2012). NO₂ also
839 reaches a maximum over Northern East China as a result of substantial anthropogenic
840 sources. From POMINO to POMINO v1.1, the NO₂ VCD increases by 3.4% (-67.5–
841 41.7%) in spring for the domain average (range), 3.0% (-59.5–34.4%) in summer, 4.6%
842 (-15.3–39.6%) in fall and 5.3% (-68.4–49.3%) in winter. The NO₂ change is highly
843 dependent on the location and season. The increase over Northern East China is
844 largest in winter, wherein the positive value for ΔALH implies that elevated aerosol
845 layers “shield” the NO₂ absorption.

846 6. Evaluating satellite products using MAX-DOAS data

847 We use MAX-DOAS data, after cloud screening (Sect. 2.4), to evaluate DOMNO v2,
848 QA4ECV, POMINO and POMINO v1.1. The scatterplots in Fig. 9a-d compare the
849 NO₂ VCDs from 162 OMI pixels on 49 days with their MAX-DOAS counterparts.
850 Different colors differentiate the seasons. The high values of NO₂ VCD ($> 30 \times 10^{15}$
851 molec. cm⁻²) occur mainly in fall (blue) and winter (black). POMINO v1.1 and
852 POMINO capture the day-to-day variability of MAX-DOAS data, i.e., $R^2 = 0.804$ and
853 0.799, respectively. The normalized mean bias (NMB) of POMINO v1.1 relative to

删除的内容: 7

删除的内容: 9

删除的内容: mean

删除的内容: that better

删除的内容: 10a-c

859 MAX-DOAS data (-3.4%) is smaller than the NMB of POMINO (-9.6%). Also, the
860 reduced major axis (RMA) regression shows that the slope for POMINO v1.1 (0.95)
861 is closer to unity than the slope for POMINO (0.78). When all OMI pixels in a day are
862 averaged (Fig. 9e), the correlation across the total of 49 days further increase for
863 both POMINO v1.1 ($R^2 = 0.89$) and POMINO ($R^2 = 0.86$), whereas POMINO v1.1
864 still has a lower NMB (-3.7%) and better slope (0.96) than POMINO (-10.4% and
865 0.82, respectively). These results suggest that correcting aerosol vertical profiles, at
866 least on a climatology basis, already leads to a significant improved NO_2 retrieval
867 from OMI.

868 Figure 9 shows that DOMINO v2 is correlated with MAX-DOAS ($R^2 = 0.68$ in Fig.
869 9c and 0.75 in Fig. 9e) but not as strong as POMINO and POMINO v1.1 for all days.
870 The discrepancy between DOMINO v2 and MAX-DOAS is particularly large for very
871 high NO_2 values ($> 70 \times 10^{15}$ molec. cm^{-2}). The R^2 for QA4ECV (0.75 in Fig. 9d
872 and 0.82 in Fig. 9h) is slightly better than DOMINO, but the NMB is higher (-22.0%
873 and -22.7%) and the slope drops to 0.66. These results are consistent with the finding
874 of Lin et al. (2014b, 2015) that explicitly including aerosol optical effects improves
875 the NO_2 retrieval.

876 Table 2 further shows the comparison statistics for 27 haze days. The haze days are
877 determined when both the ground meteorological station data and MODIS/Aqua
878 corrected reflectance (true color) data indicate a haze day. The table also lists AOD,
879 SSA, CF and MAX-DOAS NO_2 VCD, as averaged over all haze days. A large
880 amount of absorbing aerosols occurs on these haze days (AOD = 1.13, SSA = 0.90).
881 The average MAX-DOAS NO_2 VCD reaches 51.92×10^{15} molec. cm^{-2} . Among the
882 four satellite products, POMINO v1.1 has the highest R^2 (0.76) and the lowest bias
883 (4.4%) with respect to MAX-DOAS, whereas DOMINO v2 and QA4ECV reproduce
884 the variability to a limited extent ($R^2 = 0.38$ and 0.34, respectively). This is consistent

删除的内容: 11d,e

删除的内容:

批注 [FB3]: Please clarify if this is now for haze days, or all days.

删除的内容: 10c,f

删除的内容: 10

删除的内容: 45

删除的内容: 10

删除的内容: f

删除的内容: well

带格式的: 上标

删除的内容: much

删除的内容: 4

删除的内容: three

删除的内容: s

897 with the previous finding that the accuracy of DOMINO v2 is reduced for polluted,
898 aerosol-loaded scenes (Boersma et al., 2011; Chimot et al., 2016; Kanaya et al., 2014;
899 Lin et al., 2014b).

删除的内容: c

900 Table 3 shows the comparison statistics for 36 cloud-free days (CF = 0 in POMINO,
901 and AOD = 0.60 on average). Here, POMINO v1.1, POMINO and DONIMO v2 do
902 not show large differences in R^2 (0.53–0.56) and NMB (20.8–29.4%), with respect to
903 MAX-DOAS. QA4ECV has a higher R^2 (0.63) and a lower NMB (-5.83%),
904 presumably reflecting the improvements in this community best practices approach, at
905 least in mostly cloud-free situations. However, the R^2 values for POMINO and
906 POMINO v1.1 are much smaller than the R^2 values in haze days, whereas the
907 opposite changes are true for DOMINO v2 and QA4ECV. Thus, for this limited set of
908 data, the changes from DOMINO v2 and QA4ECV to POMINO and POMINO v1.1
909 mainly reflect the improved aerosol treatment in hazy scenes. Further research may
910 use additional MAX-DOAS datasets to evaluate the satellite products more
911 systematically.

带格式的: 段落间距段后: 10 磅, 图案: 清除

删除的内容: 5

删除的内容: the three OMI products

删除的内容: and NMB (20.8–29.4%)

带格式的: 字体: (中文) + 中文正文 (宋体), 上标

删除的内容: that in the cloud-free cases the ensemble of algorithms improves the retrieval results

删除的内容: is

912 7. Conclusions

913 This paper improves upon our previous POMINO algorithm (Lin et al., 2015) to
914 retrieve the tropospheric NO₂ VCDs from OMI, by compiling a 9-year (2007–2015)
915 CALIOP monthly climatology of aerosol vertical extinction profiles to adjust
916 GEOS-Chem aerosol profiles used in the NO₂ retrieval process. The improved
917 algorithm is referred to as POMINO v1.1. Compared to monthly climatological
918 CALIOP data over China, GEOS-Chem simulations tend to underestimate the aerosol
919 extinction above 1 km, as characterized by an underestimate in ALH by 300–600 m
920 (seasonal and location dependent). Such a bias is corrected in POMINO v1.1 by
921 dividing, for any month and grid cell, the CALIOP monthly climatological profile by

删除的内容: ↵

删除的内容: product

931 the model climatological profile to obtain a scaling profile and then applying the
932 scaling profile to model data in all days of that month in all years.

933 The aerosol extinction profile correction leads to an insignificant change in CF from
934 POMINO to POMINO v1.1, since the AOD and surface reflectance are unchanged. In
935 contrast, the correction results in a notably increase in CP (i.e., a decrease in CTH),
936 due to lifting of aerosol layers. The CP changes are generally within 6% for scenes
937 with low cloud fraction ($CF < 0.05$ in POMINO), and within 2% for scenes with
938 modest cloud fraction ($0.2 < CF < 0.3$ in POMINO).

939 The NO_2 VCDs increase from POMINO to POMINO v1.1 in most cases due to lifting
940 of aerosol layers that enhances the “shielding” of NO_2 absorption. The NO_2 VCD
941 increases by 3.4% (-67.5–41.7%) in spring for the domain average (range), 3.0%
942 (-59.5–34.4%) in summer, 4.6% (-15.3–39.6%) in fall and 5.3% (-68.4–49.3%) in
943 winter. The NO_2 changes highly season and location dependent, and are most
944 significant for wintertime Northern East China.

945 Further comparisons with independent MAX-DOAS NO_2 VCD data for 162 OMI
946 pixels in 49 days show good performance of both POMINO v1.1 and POMINO in
947 capturing the day-to-day variation of NO_2 ($R^2=0.80$, $n=162$), compared to DOMINO
948 v2 ($R^2=0.67$) and the new QA4ECV product ($R^2=0.75$). The NMB is smaller in
949 POMINO v1.1 (-3.4%) than in POMINO (-9.6%), with a slightly better slope (0.804
950 versus 0.784). On hazy days with high aerosol loadings ($AOD = 1.13$ on average),
951 POMINO v1.1 has the highest R^2 (0.76) and the lowest bias (4.4%) whereas
952 DOMINO and QA4ECV have difficulty in reproducing the day-to-day variability in
953 MAX-DOAS NO_2 measurements ($R^2 = 0.38$ and 0.34 , respectively). The four
954 products show small differences in R^2 on clear-sky days ($CF = 0$ in POMINO, $AOD =$
955 0.60 on average). Thus the explicit aerosol treatment (in POMINO and POMINO v1.1)

删除的内容: or

删除的内容: has

删除的内容: ,

删除的内容: three

删除的内容: and NMB

961 and the aerosol vertical profile correction (in POMINO v1.1) improves the NO₂
962 retrieval especially in hazy cases.

963 [The POMINO v1.1 algorithm is a core step towards our next public release of data](#)
964 [product, POMINO v2. This new release will contain a few additional updates,](#)
965 [including but not limited to using MODIS Collection 6 Merged 10-km Level-2 AOD](#)
966 [data that combine the Dark Target \(Levy et al., 2013\) and Deep Blue \(Sayer et al.,](#)
967 [2014\) products, as well as MODIS MCD43C2 Collection 6 daily BRDF data.](#)
968 [Meanwhile, the POMINO algorithm framework is being applied to the recently](#)
969 [launched TropOMI instrument that provides NO₂ information at a much higher spatial](#)
970 [resolution \(3.5 x 7 km²\). A modified algorithm can also be used to retrieve sulfur](#)
971 [dioxide, formaldehyde and other trace gases from TropOMI, for which purposes our](#)
972 [algorithm will be available to the community on a collaborative basis. Future research](#)
973 [can correct the SSA and NO₂ vertical profile to further improve the retrieval](#)
974 [algorithm, and can use more comprehensive independent data to evaluate the resulting](#)
975 [satellite products.](#)

976 Acknowledgements

977 This research is supported by the National Natural Science Foundation of China
978 (41775115), the 973 program (2014CB441303), the Chinese Scholarship Council, and
979 the EU FP7 QA4ECV project (grant no. 607405).

980 Appendix A: Introduction to the QA4ECV product

981 [The QA4ECV NO₂ product \(http://www.qa4ecv.eu/\)](#) builds on a (EU-) consortium
982 [best practices approach to retrieve NO₂ from GOME, SCIAMACHY, GOME-2, and](#)
983 [OMI. The main contributions are provided by BIRA-IASB, the University of Bremen](#)
984 [\(IUP\), MPIC, KNMI, and Wageningen University. Uncertainties in spectral fitting for](#)
985 [NO₂ SCDs and in AMF calculations were evaluated by Zara et al. \(2018\) and Lorente](#)

删除的内容:

删除的内容: KFB: I think a sentence on the relatively good performance of QA4ECV in non-hazy days would be useful. Your paper adds value to the literature by being one of the first to do a systematic validation of the QA4ECV product! You have already some good indications when the algorithm does fine, and under which circumstances it is biased. This should be highlighted.

删除的内容: (Levy et al., 2013)

批注 [JL4]: citation

删除的内容: (Sayer et al., 2013)

删除的内容: Our POMINO v1.1

删除的内容: ↵

带格式的

带格式的: 标题 1, 左, 段落间距段后: 0 磅, 图案: 清除

删除的内容: The

删除的内容: i

带格式的

带格式的

带格式的: 字体: 非加粗

删除的内容: EU FP7-project Quality Assurance for Essential ... [5]

删除的内容:)

删除的内容: is aim at making rapid judgments on validity and ... [6]

删除的内容: is

带格式的: 字体: 非加粗

带格式的: 下标

删除的内容: a kind of

删除的内容: essentially an ensemble data sets of satellite products ... [7]

删除的内容: and

删除的内容: , with a fully traceable quality assurance on all aspects ... [8]

带格式的: 下标

删除的内容: The u

删除的内容: of

删除的内容: algorithms

删除的内容: the

带格式的: 下标

删除的内容: ,

1021 et al., (2017), respectively. QA4ECV contains improved SCD NO₂ data (Zara et al.,
 1022 2018). Lorente et al., (2017) showed that across the above algorithms, there a
 1023 structural uncertainty by 42% in the NO₂ AMF calculation over polluted areas. By
 1024 comparing to our POMINO product, Lorente et al. also showed that the choice of
 1025 aerosol correction may introduce an additional uncertainty by up to 50% for situations
 1026 with high polluted cases, consistent with [Lin et al. (2014b, 2015)] and the findings
 1027 here. For a complete description of the QA4ECV algorithm improvements, and
 1028 quality assurance, please see Boersma et al. (2018).

1029 **Appendix B: Constructing the CALIOP monthly climatology of aerosol**
 1030 **extinction vertical profile.**

1031 Our use the all-sky Level-2 CALIOP data to construct the Level-3 monthly
 1032 climatology. We choose the all-sky product instead of clear-sky data, since previous
 1033 studies indicate that the climatological aerosol extinction profiles are affected
 1034 insignificantly by the presence of clouds (Koffi et al., 2012; Winker et al., 2013). As
 1035 we use this climatological data to adjust GEOS-Chem results, choosing all-sky data
 1036 improves consistency with the model simulation when doing the daily correction.

1037 To select valid pixels, we follow the data quality criteria by Winker et al., (2013) and
 1038 Amiridis et al., (2015). Only the pixels with Cloud Aerosol Discrimination (CAD)
 1039 scores between -20 and -100 with extinction Quality Control (QC) flag valued at 0, 1,
 1040 18, and 16 are selected. We further discard samples with an extinction uncertainty of
 1041 99.9 km⁻¹, which is indicative of unreliable retrieval. We only accept extinction values
 1042 falling in the range from 0.0 to 1.25, according to CALIOP observation thresholds.
 1043 Previous studies showed that weakly scattering edges of icy clouds are sometimes
 1044 misclassified as aerosols (Winker et al., 2013). To eliminate contamination from icy
 1045 clouds we exclude the aerosol layers above the cloud layer (with layer-top
 1046 temperature below 0 °C) when both of them are above 4km (Winker et al., 2013).

- 删除的内容: ,
- 删除的内容: The improved
- 删除的内容: NO₂
- 带格式的: 下标
- 删除的内容: shows better performance in
- 删除的内容: but do not altogether eliminated systematic errors in ththee fitting approach
- 删除的内容: 42%
- 删除的内容: of
- 带格式的: 下标
- 删除的内容: s
- 删除的内容: aereas
- 删除的内容: , and
- 删除的内容: s
- 删除的内容: average
- 删除的内容: of
- 批注 [JL5]: Revise the format of the reference list
- 带格式的: 荷兰语
- 删除的内容:
- 带格式的
- 删除的内容: The way to c
- 带格式的
- 带格式的
- 删除的内容: mean
- 带格式的
- 带格式的
- 带格式的
- 删除的内容: climatology
- 带格式的: 字体: 非加粗
- 已移动(插入) [5]
- 删除的内容: The way to select the good quality profile mainly
- 删除的内容: s
- 已移动(插入) [1]

1068 [After the pixel-based screening, we aggregate the CALIOP data at the model grid](#)
1069 [\(0.667° long. x 0.5° lat.\) and vertical resolution \(47 layers, with 36 layers or so in the](#)
1070 [troposphere\). For each grid cell, we choose the CALIOP pixels within 1.5° of the grid](#)
1071 [cell center. CALIOP Level-2 data are always presented at the fixed 399 altitudes](#)
1072 [above sea level. To account for the difference in surface elevation between a CALIOP](#)
1073 [pixel and the respective model grid cell, we convert the altitude of the pixel to a](#)
1074 [height above the ground, by using the surface elevation data provided in CALIOP.](#)
1075 [We then average horizontally and vertically the profiles of all pixels within one model](#)
1076 [grid cell and layer. We do the regridding day-by-day for all grid cells to ensure that](#)
1077 [GEOS-Chem and CALIOP extinction profiles are coincident spatially and temporally.](#)
1078 [Finally, we compile a monthly climatological dataset by averaging over 2007–2015.](#)

已移动(插入) [2]

1079 [Figure A1 shows the number of aerosol extinction profiles in each grid cell and 12 x 9](#)
1080 [= 108 months that are used to compile the CALIOP climatology, both before and after](#)
1081 [data screening. Table A1 presents additional information on monthly and yearly bases.](#)
1082 [On average, there are 165 and 47 aerosol extinction profiles per month per grid cell](#)
1083 [before and after screening, respectively. In the final 9-year monthly climatology, each](#)
1084 [grid cell has about 420 aerosol extinction profiles on average, about 28% of the](#)
1085 [prior-screening profiles. Figure A1 shows that the number of valid profiles decreases](#)
1086 [sharply over the Tibet Plateau and at higher latitudes \(> 43° N\) due to complex](#)
1087 [terrain and icy/snowy ground.](#)

删除的内容: ↵

已移动(插入) [3]

1088 [As discussed above, we choose the CALIOP pixels within 1.5° of a grid cell center.](#)
1089 [We test this choice by examining the aerosol layer height \(ALH\) produced for that](#)
1090 [grid cell. The ALH is defined as the extinction-weighted height of aerosols \(see Eq.](#)
1091 [A1, where \$n\$ denotes the number of tropospheric layers, \$\epsilon_i\$ the aerosol extinction at](#)
1092 [layer \$i\$, and \$H_i\$ the layer center height above the ground\). We find that choosing](#)
1093 [pixels within 1.0° of a grid cell center leads to a nosier horizontal distribution of](#)

1095 ALH, owing to the small footprint of CALIOP. On the other hand, choosing 2.0°
1096 leads to a too smooth spatial gradient of ALH with local characteristics of aerosol
1097 vertical distributions are largely lost. We thus decide that 1.5° is a good balance
1098 between noise and smoothness.

$$1099 \text{ ALH} = \frac{\sum_{i=1}^{i=n} \epsilon_i H_i}{\sum_{i=1}^{i=n} \epsilon_i} \quad (\text{A1})$$

1100 Certain grid cells do not contain sufficient valid observations for some months of the
1101 climatological dataset. We fill in missing monthly values of a grid cell using valid
1102 data in the surrounding $5 \times 5 = 25$ grid cells (within ~ 100 km). If the 25 grid cells do
1103 not have enough valid data, we use those in the surrounding $7 \times 7 = 49$ grid cells
1104 (within ~ 150 km). A similar procedure is used by Lin et al. (2014b, 2015) to fill in
1105 missing values in the gridded MODIS AOD dataset.

1106 ~~For each grid cell in each month, we further correct singular values in the vertical~~
1107 ~~profile. In a month, if a grid cell i has an ALH outside $\text{mean} \pm 1 \sigma$ of its surrounding~~
1108 ~~25 or 49 grid cells, we select i 's surrounding grid cell j whose ALH is the median of~~
1109 ~~i 's surrounding grid cells, and use j 's profile to replace i 's. Whether 25 or 49~~
1110 ~~surrounding grid cells are chosen depends on the number of valid pixels shown in Fig.~~
1111 ~~A1b. If the number of valid pixels in i is below $\text{mean} - 1 \sigma$ of all grid cells in the whole~~
1112 ~~domain, which is often the case for Tibetan grid cells, we use i 's surrounding 49 grid~~
1113 ~~cells; otherwise we use i 's surrounding 25 grid cells.~~

1114 **Appendix C. Comparing our and NASA's CALIOP monthly climatology**

1115 We compare our gridded climatological profiles to NASA CALIOP Version 3
1116 Level-3 all-sky monthly profiles at 532 nm (Winker et al., 2013). The NASA Level-3
1117 data has a horizontal resolution of 2° lat. \times 5° lon. and a vertical resolution of 60
1118 m (from -0.5 to 12 km above sea level). We combine NASA monthly data over 2007–

删除的内容: Certain grid cells do not contain sufficient valid observations for some months of the climatological data set. We fill in missing monthly values of a grid cell using valid data in the surrounding 25 or 49 grid cells.

已移动(插入) [4]

带格式的: 字体: 非加粗

带格式的: 字体: 非加粗

带格式的: 标题 1

1123 [2015 to construct a monthly climatology for comparison with our own compilation.](#)
1124 [We only choose aerosol extinction data in the troposphere with error less than 0.15](#)
1125 [\(the valid range given in the CALIOP dataset\). If the number of valid monthly](#)
1126 [profiles in a grid cell is less than five \(i.e., for the same month in five out of the nine](#)
1127 [years\), then we exclude data in that grid cell; see the dark gray grid cells in Fig. 2c.](#)

1128 [Several methodological differences exist between generating our and NASA CALIOP](#)
1129 [datasets. First, the two datasets have different horizontal resolutions. Also, we sample](#)
1130 [all valid CALIOP pixels within 1.5° of a grid cell center, whereas the NASA dataset](#)
1131 [samples all valid pixels within a grid cell. Besides, our CALIOP dataset involves](#)
1132 [several steps of horizontal interpolation, for purposes of subsequent cloud and NO₂](#)
1133 [retrievals, which is not done in the NASA dataset. In addition, we match CALIOP](#)
1134 [data vertically to the GEOS-Chem vertical resolution, whereas the NASA dataset](#)
1135 [maintains the original resolution.](#)

1136 [Figure 2c shows the spatial distribution of ALH in all seasons based on NASA](#)
1137 [CALIOP Level-3 all-sky monthly climatology. The horizontal resolution of NASA](#)
1138 [data is much coarser than ours; and NASA data are largely missing over the southwest](#)
1139 [with complex terrains. We choose to focus on the comparison over East China \(the](#)
1140 [black box in Fig. 1a\). Over East China, the two climatology datasets generally exhibit](#)
1141 [similar spatial patterns of ALH in all seasons \(Fig. 2a, c\). The NASA dataset suggests](#)
1142 [higher ALHs than ours over Eastern China, especially in summer, due mainly to](#)
1143 [differences in the sampling and regridding processes. Figure 3c further compares the](#)
1144 [monthly variation of ALH between our \(black line with error bars\) and NASA \(blue](#)
1145 [filled triangles\) datasets averaged over East China. The two datasets are consistent in](#)
1146 [almost all months, indicating that their regional differences are largely smoothed out](#)
1147 [by spatial averaging.](#)

1148 **References**

带格式的: 图案: 清除

带格式的: 字体: 非加粗

删除的内容: Appendix C: The introduction to new version of POMINO product^d

In our new released version, several aspect will be update:^d

1) Use 9-year CALIOP climatology aerosol extinction profile to adjust GEOS-Chem daily aerosol extinction profiles. This is the main update in our new released version, which will also be applied to the retrieval algorithm of newly laughed TropOMI sensor.^d

2) MODIS Collection 6 Merged 10-km Level-2 AOD product will be used to replace the MODIS Collection 5 Dark Target (DT) product to adjust model simulation. Previous studies has shown various contextual biases exist in C5 version (Levy et al., 2010; Bréon et al., 2011). The C6 product updates the widely used DT (Levy et al., 2013) and Deep Blue (DB) product (Sayer et al., 2013). It also released the merged AOD product to provide a more gap-filled data set based on DT, DB and MODIS-derived climatologies of NDVI (Huete et al., 2011).^d

3) MODIS MCD43C2 Collection 6 daily BRDF/Albedo Snow-free Model Parameters Daily L3 Global 0.05Deg data set is used to replace C5 8-day averaged data set to account for the daily BRDF effect of surface. There is improved quality and more retrieval at high latitudes and use current day snow status when retrieval in C6.^d

^d

^d

^d

带格式的

1175 Acarreta, J. R., De Haan, J. F. and Stammes, P.: Cloud pressure retrieval using the O₂
1176 -O₂ absorption band at 477 nm, *J. Geophys. Res.*, 109(D5), D05204,
1177 doi:10.1029/2003JD003915, 2004.

带格式的: 两端对齐

1178 Amiridis, V., Marinou, E., Tsekeri, A., Wandinger, U., Schwarz, A., Giannakaki, E.,
1179 Mamouri, R., Kokkalis, P., Biniotoglou, I., Solomos, S., Herekakis, T., Kazadzis, S.,
1180 Gerasopoulos, E., Proestakis, E., Kottas, M., Balis, D., Papayannis, A., Kontoes, C.,
1181 Kourtidis, K., Papagiannopoulos, N., Mona, L., Pappalardo, G., Le Rille, O. and
1182 Ansmann, A.: LIVAS: a 3-D multi-wavelength aerosol/cloud database based on
1183 CALIPSO and EARLINET, *Atmos. Chem. Phys.*, 15(13), 7127–7153,
1184 doi:10.5194/acp-15-7127-2015, 2015.

1185 Belmonte Rivas, M., Veeffkind, P., Boersma, F., Levelt, P., Eskes, H. and Gille, J.:
1186 Intercomparison of daytime stratospheric NO₂: satellite retrievals and model
1187 simulations, *Atmos. Meas. Tech.*, 7(7), 2203–2225, doi:10.5194/amt-7-2203-2014,
1188 2014.

删除的内容: <sub>

删除的内容: </sub>

1189 Boersma, K. F., Eskes, H. J. and Brinksma, E. J.: Error analysis for tropospheric NO₂
1190 retrieval from space, *J. Geophys. Res. Atmos.*, 109(D4), n/a-n/a,
1191 doi:10.1029/2003JD003962, 2004.

1192 Boersma, K. F., Eskes, H. J., Veeffkind, J. P., Brinksma, E. J., van der A, R. J., Sneep,
1193 M., van den Oord, G. H. J., Levelt, P. F., Stammes, P., Gleason, J. F. and Bucsela, E.
1194 J.: Near-real time retrieval of tropospheric NO₂ from OMI, *Atmos. Chem. Phys.*,
1195 7(8), 2103–2118, doi:10.5194/acp-7-2103-2007, 2007.

删除的内容: <sub>

删除的内容: </sub>

1196 Boersma, K. F., Eskes, H. J., Dirksen, R. J., van der A, R. J., Veeffkind, J. P., Stammes,
1197 P., Huijnen, V., Kleipool, Q. L., Sneep, M., Claas, J., Leitão, J., Richter, A., Zhou, Y.
1198 and Brunner, D.: An improved tropospheric NO₂: column retrieval algorithm for the

删除的内容: <sub>

删除的内容: </sub>

1205 Ozone Monitoring Instrument, Atmos. Meas. Tech., 4(9), 1905–1928,
1206 doi:10.5194/amt-4-1905-2011, 2011a.

1207 [Boersma, K.F., Eskes, H. J., Richter, A., De Smedt, I., Lorente, A., Beirle, S., van](#)
1208 [Geffen, J. H. G. M., Zara, M., Peters, E., Van Roozendael, M., Wagner, T.,](#)
1209 [Maasackers, J. D., van der A, R. J., Nightingale, J., De Rudder, A., Irie, H., and](#)
1210 [Pinardi, G.: Improving algorithms and uncertainty estimates for satellite NO₂](#)
1211 [retrievals: Results from the Quality Assurance for Essential Climate Variables](#)
1212 [\(QA4ECV\) project, amt-2018-200, submitted, 2018.](#)

1213 Bucsela, E. J., Celarier, E. A., Wenig, M. O., Gleason, J. F., Veefkind, J. P., Boersma,
1214 K. F. and Brinksma, E. J.: Algorithm for NO₂ vertical column retrieval from the
1215 ozone monitoring instrument, IEEE Trans. Geosci. Remote Sens., 44(5), 1245–1258,
1216 doi:10.1109/TGRS.2005.863715, 2006.

1217 Bucsela, E. J., Krotkov, N. A., Celarier, E. A., Lamsal, L. N., Swartz, W. H., Bhartia,
1218 P. K., Boersma, K. F., Veefkind, J. P., Gleason, J. F. and Pickering, K. E.: A new
1219 stratospheric and tropospheric NO₂ retrieval algorithm for nadir-viewing satellite
1220 instruments: applications to OMI, Atmos. Meas. Tech., 6(10), 2607–2626,
1221 doi:10.5194/amt-6-2607-2013, 2013.

1222 Castellanos, P., Boersma, K. F. and van der Werf, G. R.: Satellite observations
1223 indicate substantial spatiotemporal variability in biomass burning NO_x emission
1224 factors for South America, Atmos. Chem. Phys., 14(8), 3929–3943,
1225 doi:10.5194/acp-14-3929-2014, 2014.

1226 Castellanos, P., Boersma, K. F., Torres, O. and de Haan, J. F.: OMI tropospheric NO₂
1227 air mass factors over South America: effects of biomass burning aerosols, Atmos.
1228 Meas. Tech., 8(9), 3831–3849, doi:10.5194/amt-8-3831-2015, 2015.

删除的内容: Boersma, K. F., Eskes, H. J., Dirksen, R. J., van der A, R. J., Veefkind, J. P., Stammes, P., Huijnen, V., Kleipool, Q. L., Sneep, M., Claas, J., Leitão, J., Richter, A., Zhou, Y. and Brunner, D.: An improved tropospheric NO₂ column retrieval algorithm for the Ozone Monitoring Instrument, Atmos. Meas. Tech., 4(9), 1905–1928, doi:10.5194/amt-4-1905-2011, 2011b. KFB: cited twice.†

Boersma, K. F., Eskes, H. J., Dirksen, R. J., van der A, R. J., Veefkind, J. P., Stammes, P., Huijnen, V., Kleipool, Q. L., Sneep, M., Claas, J., Leitão, J., Richter, A., Zhou, Y. and Brunner, D.: An improved tropospheric NO₂ column retrieval algorithm for the Ozone Monitoring Instrument, Atmos. Meas. Tech., 4(9), 1905–1928, doi:10.5194/amt-4-1905-2011, 2011c. Cited thrice.

删除的内容: /sub

删除的内容: /

删除的内容: <sub>

删除的内容: <sub>

删除的内容: <sub>

删除的内容: <sub>

删除的内容: <sub>

删除的内容: <sub>

1251 Chazette, P., Raut, J.-C., Dulac, F., Berthier, S., Kim, S.-W., Royer, P., Sanak, J.,
1252 Loaëc, S. and Grigaut-Desbrosses, H.: Simultaneous observations of lower
1253 tropospheric continental aerosols with a ground-based, an airborne, and the
1254 spaceborne CALIOP lidar system, *J. Geophys. Res.*, 115(D4), D00H31,
1255 doi:10.1029/2009JD012341, 2010.

1256 Chimot, J., Vlemmix, T., Veefkind, J. P., de Haan, J. F. and Levelt, P. F.: Impact of
1257 aerosols on the OMI tropospheric NO₂ retrievals over industrialized regions: how
1258 accurate is the aerosol correction of cloud-free scenes via a simple cloud model?,
1259 *Atmos. Meas. Tech.*, 9(2), 359–382, doi:10.5194/amt-9-359-2016, 2016.

1260 Clémer, K., Van Roozendaal, M., Fayt, C., Hendrick, F., Hermans, C., Pinardi, G.,
1261 Spurr, R., Wang, P. and De Mazière, M.: Multiple wavelength retrieval of
1262 tropospheric aerosol optical properties from MAXDOAS measurements in Beijing,
1263 *Atmos. Meas. Tech.*, 3(4), 863–878, doi:10.5194/amt-3-863-2010, 2010.

1264 Cui, Y., Lin, J., Song, C., Liu, M., Yan, Y., Xu, Y. and Huang, B.: Rapid growth in
1265 nitrogen dioxide pollution over Western China, 2005–2013, *Atmos. Chem. Phys.*,
1266 16(10), 6207–6221, doi:10.5194/acp-16-6207-2016, 2016.

1267 Dirksen, R. J., Boersma, K. F., Eskes, H. J., Ionov, D. V., Bucsela, E. J., Levelt, P. F.
1268 and Kelder, H. M.: Evaluation of stratospheric NO₂ retrieved from the Ozone
1269 Monitoring Instrument: Intercomparison, diurnal cycle, and trending, *J. Geophys.*
1270 *Res.*, 116(D8), D08305, doi:10.1029/2010JD014943, 2011.

1271 van Geffen, J. H. G. M., Boersma, K. F., Van Roozendaal, M., Hendrick, F., Mahieu,
1272 E., De Smedt, I., Sneep, M. and Veefkind, J. P.: Improved spectral fitting of nitrogen
1273 dioxide from OMI in the 405–465 nm window, *Atmos. Meas. Tech.*, 8(4), 1685–1699,
1274 doi:10.5194/amt-8-1685-2015, 2015.

删除的内容: <sub>

删除的内容: </sub>

1277 Gielen, C., Van Roozendaal, M., Hendrick, F., Pinardi, G., Vlemmix, T., De Bock, V.,
1278 De Backer, H., Fayt, C., Hermans, C., Gillotay, D. and Wang, P.: A simple and
1279 versatile cloud-screening method for MAX-DOAS retrievals, *Atmos. Meas. Tech.*,
1280 7(10), 3509–3527, doi:10.5194/amt-7-3509-2014, 2014.

1281 Huang, Z., Huang, J., Bi, J., Wang, G., Wang, W., Fu, Q., Li, Z., Tsay, S.-C. and Shi,
1282 J.: Dust aerosol vertical structure measurements using three MPL lidars during 2008
1283 China-U.S. joint dust field experiment, *J. Geophys. Res. Atmos.*, 115(D7), n/a-n/a,
1284 doi:10.1029/2009JD013273, 2010.

1285 Irie, H., Boersma, K. F., Kanaya, Y., Takashima, H., Pan, X. and Wang, Z. F.:
1286 Quantitative bias estimates for tropospheric NO₂ columns retrieved from
1287 SCIAMACHY, OMI, and GOME-2 using a common standard for East Asia, *Atmos.*
1288 *Meas. Tech.*, 5(10), 2403–2411, doi:10.5194/amt-5-2403-2012, 2012.

删除的内容: <sub>

删除的内容: <sub>

1289 Johnson, M. S., Meskhidze, N. and Praju Kiliyanpilakkil, V.: A global comparison of
1290 GEOS-Chem-predicted and remotely-sensed mineral dust aerosol optical depth and
1291 extinction profiles, *J. Adv. Model. Earth Syst.*, 4(3), M07001,
1292 doi:10.1029/2011MS000109, 2012.

1293 Kacenelenbogen, M., Redemann, J., Vaughan, M. A., Omar, A. H., Russell, P. B.,
1294 Burton, S., Rogers, R. R., Ferrare, R. A. and Hostetler, C. A.: An evaluation of
1295 CALIOP/CALIPSO's aerosol-above-cloud detection and retrieval capability over
1296 North America, *J. Geophys. Res. Atmos.*, 119(1), 230–244,
1297 doi:10.1002/2013JD020178, 2014.

1298 Kanaya, Y., Irie, H., Takashima, H., Iwabuchi, H., Akimoto, H., Sudo, K., Gu, M.,
1299 Chong, J., Kim, Y. J., Lee, H., Li, A., Si, F., Xu, J., Xie, P.-H., Liu, W.-Q., Dzhola, A.,
1300 Postlyakov, O., Ivanov, V., Grechko, E., Terpugova, S. and Panchenko, M.:
1301 Long-term MAX-DOAS network observations of NO₂ in Russia and Asia (MADRAS)

删除的内容: <sub>

删除的内容: <sub>

1306 during the period 2007–2012: instrumentation, elucidation of climatology, and
1307 comparisons with OMI satellite observations and global model simulations, *Atmos.*
1308 *Chem. Phys.*, 14(15), 7909–7927, doi:10.5194/acp-14-7909-2014, 2014.

删除的内容: &ndash;

1309 Kim, S.-W., Heckel, A., Frost, G. J., Richter, A., Gleason, J., Burrows, J. P., McKeen,
1310 S., Hsie, E.-Y., Granier, C. and Trainer, M.: NO₂ columns in the western United
1311 States observed from space and simulated by a regional chemistry model and their
1312 implications for NO_x emissions, *J. Geophys. Res.*, 114(D11), D11301,
1313 doi:10.1029/2008JD011343, 2009.

1314 Koffi, B., Schulz, M., Bréon, F.-M., Griesfeller, J., Winker, D., Balkanski, Y., Bauer,
1315 S., Bernsten, T., Chin, M., Collins, W. D., Dentener, F., Diehl, T., Easter, R., Ghan, S.,
1316 Ginoux, P., Gong, S., Horowitz, L. W., Iversen, T., Kirkevåg, A., Koch, D., Krol, M.,
1317 Myhre, G., Stier, P. and Takemura, T.: Application of the CALIOP layer product to
1318 evaluate the vertical distribution of aerosols estimated by global models: AeroCom
1319 phase I results, *J. Geophys. Res. Atmos.*, 117(D10), n/a-n/a,
1320 doi:10.1029/2011JD016858, 2012.

1321 Leitão, J., Richter, A., Vrekoussis, M., Kokhanovsky, A., Zhang, Q. J., Beekmann, M.
1322 and Burrows, J. P.: On the improvement of NO₂ satellite retrievals – aerosol impact
1323 on the airmass factors, *Atmos. Meas. Tech.*, 3(2), 475–493,
1324 doi:10.5194/amt-3-475-2010, 2010.

删除的内容: <sub>

删除的内容: </sub>

1325 Lerot, C., Stavrakou, T., De Smedt, I., Müller, J.-F. and Van Roozendael, M.: Glyoxal
1326 vertical columns from GOME-2 backscattered light measurements and comparisons
1327 with a global model, *Atmos. Chem. Phys.*, 10(24), 12059–12072,
1328 doi:10.5194/acp-10-12059-2010, 2010.

1332 Levy, R. C., Mattoo, S., Munchak, L. A., Remer, L. A., Sayer, A. M., Patadia, F. and
1333 Hsu, N. C.: The Collection 6 MODIS aerosol products over land and ocean, *Atmos.*
1334 *Meas. Tech.*, 6(11), 2989–3034, doi:10.5194/amt-6-2989-2013, 2013.

1335 Li, S., Yu, C., Chen, L., Tao, J., Letu, H., Ge, W., Si, Y. and Liu, Y.:
1336 Inter-comparison of model-simulated and satellite-retrieved componential aerosol
1337 optical depths in China, *Atmos. Environ.*, 141, 320–332,
1338 doi:https://doi.org/10.1016/j.atmosenv.2016.06.075, 2016.

1339 Lin, J., Pan, D., Davis, S. J., Zhang, Q., He, K., Wang, C., Streets, D. G., Wuebbles,
1340 D. J. and Guan, D.: China's international trade and air pollution in the United States,
1341 *Proc. Natl. Acad. Sci.*, 111(5), 1736–1741, doi:10.1073/pnas.1312860111, 2014a.

1342 Lin, J.-T.: Satellite constraint for emissions of nitrogen oxides from anthropogenic,
1343 lightning and soil sources over East China on a high-resolution grid, *Atmos. Chem.*
1344 *Phys.*, 12(6), 2881–2898, doi:10.5194/acp-12-2881-2012, 2012.

1345 Lin, J.-T., McElroy, M. B. and Boersma, K. F.: Constraint of anthropogenic NO_x,
1346 emissions in China from different sectors: a new methodology using multiple satellite
1347 retrievals, *Atmos. Chem. Phys.*, 10(1), 63–78, doi:10.5194/acp-10-63-2010, 2010.

1348 Lin, J.-T., Martin, R. V., Boersma, K. F., Sneep, M., Stammes, P., Spurr, R., Wang, P.,
1349 Van Roozendaal, M., Clémer, K. and Irie, H.: Retrieving tropospheric nitrogen
1350 dioxide from the Ozone Monitoring Instrument: effects of aerosols, surface
1351 reflectance anisotropy, and vertical profile of nitrogen dioxide, *Atmos. Chem. Phys.*,
1352 14(3), 1441–1461, doi:10.5194/acp-14-1441-2014, 2014b.

1353 Lin, J.-T., Liu, M.-Y., Xin, J.-Y., Boersma, K. F., Spurr, R., Martin, R. and Zhang, Q.:
1354 Influence of aerosols and surface reflectance on satellite NO₂ retrieval: seasonal and
1355 spatial characteristics and implications for NO_x emission constraints, *Atmos. Chem.*
1356 *Phys.*, 15(19), 11217–11241, doi:10.5194/acp-15-11217-2015, 2015.

删除的内容: <sub>

删除的内容: </sub>

1359 Lorente, A., Folkert Boersma, K., Yu, H., Dörner, S., Hilboll, A., Richter, A., Liu, M.,
1360 Lamsal, L. N., Barkley, M., De Smedt, I., Van Roozendael, M., Wang, Y., Wagner, T.,
1361 Beirle, S., Lin, J.-T., Krotkov, N., Stammes, P., Wang, P., Eskes, H. J. and Krol, M.:
1362 Structural uncertainty in air mass factor calculation for NO_2 and HCHO satellite retrievals,
1363 Atmos. Meas. Tech., 10(3), 759–782, doi:10.5194/amt-10-759-2017, 2017.

1364 Lucht, W., Schaaf, C. B. and Strahler, A. H.: An algorithm for the retrieval of albedo
1365 from space using semiempirical BRDF models, IEEE Trans. Geosci. Remote Sens.,
1366 38(2), 977–998, doi:10.1109/36.841980, 2000.

1367 Ma, J. Z., Beirle, S., Jin, J. L., Shaiganfar, R., Yan, P. and Wagner, T.: Tropospheric
1368 NO_2 vertical column densities over Beijing: results of the first three years of
1369 ground-based MAX-DOAS measurements (2008–2011) and satellite
1370 validation, Atmos. Chem. Phys., 13(3), 1547–1567, doi:10.5194/acp-13-1547-2013,
1371 2013.

1372 Ma, X. and Yu, F.: Seasonal variability of aerosol vertical profiles over east US and
1373 west Europe: GEOS-Chem/APM simulation and comparison with CALIPSO
1374 observations, Atmos. Res., 140–141, 28–37,
1375 doi:https://doi.org/10.1016/j.atmosres.2014.01.001, 2014.

1376 Martin, R. V.: An improved retrieval of tropospheric nitrogen dioxide from GOME, J.
1377 Geophys. Res., 107(D20), 4437, doi:10.1029/2001JD001027, 2002.

1378 Misra, A., Tripathi, S. N., Kaul, D. S. and Welton, E. J.: Study of MPLNET-Derived
1379 Aerosol Climatology over Kanpur, India, and Validation of CALIPSO Level 2
1380 Version 3 Backscatter and Extinction Products, J. Atmos. Ocean. Technol., 29(9),
1381 1285–1294, doi:10.1175/JTECH-D-11-00162.1, 2012.

删除的内容: NO_2

删除的内容: NO_2

删除的内容: NO_2

1385 Miyazaki, K. and Eskes, H.: Constraints on surface NO_x emissions by assimilating
1386 satellite observations of multiple species, *Geophys. Res. Lett.*, 40(17), 4745–4750,
1387 doi:10.1002/grl.50894, 2013.

删除的内容: x

1388 Proestakis, E., Amiridis, V., Marinou, E., Georgoulas, A. K., Solomos, S., Kazadzis,
1389 S., Chimot, J., Che, H., Alexandri, G., Biniotoglou, I., Kourtidis, K. A., de Leeuw, G.
1390 and van der A, R. J.: 9-year spatial and temporal evolution of desert dust aerosols over
1391 South-East Asia as revealed by CALIOP, *Atmos. Chem. Phys. Discuss.*, 1–35,
1392 doi:10.5194/acp-2017-797, 2017.

1393 Richter, A., Begoin, M., Hilboll, A. and Burrows, J. P.: An improved NO₂ retrieval
1394 for the GOME-2 satellite instrument, *Atmos. Meas. Tech.*, 4(6), 1147–1159,
1395 doi:10.5194/amt-4-1147-2011, 2011.

删除的内容: <sub>

删除的内容: </sub>

1396 Sareen, N., Schwier, A. N., Shapiro, E. L., Mitroo, D. and McNeill, V. F.: Secondary
1397 organic material formed by methylglyoxal in aqueous aerosol mimics, *Atmos. Chem.
1398 Phys.*, 10(3), 997–1016, doi:10.5194/acp-10-997-2010, 2010.

1399 Sayer, A. M., Munchak, L. A., Hsu, N. C., Levy, R. C., Bettenhausen, C. and Jeong,
1400 M.-J.: MODIS Collection 6 aerosol products: Comparison between Aqua’s e-Deep
1401 Blue, Dark Target, and “merged” data sets, and usage recommendations, *J. Geophys.
1402 Res. Atmos.*, 119(24), 13,965–13,989, doi:10.1002/2014JD022453, 2014.

1403 Stammes, P., Sneep, M., de Haan, J. F., Veefkind, J. P., Wang, P. and Levelt, P. F.:
1404 Effective cloud fractions from the Ozone Monitoring Instrument: Theoretical
1405 framework and validation, *J. Geophys. Res.*, 113(D16), D16S38,
1406 doi:10.1029/2007JD008820, 2008.

1407 Stavrakou, T., Müller, J.-F., Bauwens, M., De Smedt, I., Lerot, C., Van Roozendael,
1408 M., Coheur, P.-F., Clerbaux, C., Boersma, K. F., van der A, R. and Song, Y.:
1409 Substantial Underestimation of Post-Harvest Burning Emissions in the North China

1413 Plain Revealed by Multi-Species Space Observations, *Sci. Rep.*, 6, 32307,
1414 doi:10.1038/srep32307, 2016.

1415 Veefkind, J. P., de Haan, J. F., Sneep, M. and Levelt, P. F.: Improvements to the OMI
1416 O₂-O₂ operational cloud algorithm and comparisons with ground-based radar-lidar
1417 observations, *Atmos. Meas. Tech.*, 9(12), 6035–6049, doi:10.5194/amt-9-6035-2016,
1418 2016.

1419 Verstraeten, W. W., Neu, J. L., Williams, J. E., Bowman, K. W., Worden, J. R. and
1420 Boersma, K. F.: Rapid increases in tropospheric ozone production and export from
1421 China, *Nat. Geosci.*, 8, 690 [online] Available from:
1422 <http://dx.doi.org/10.1038/ngeo2493>, 2015.

1423 Wang, J., Jacob, D. J. and Martin, S. T.: Sensitivity of sulfate direct climate forcing to
1424 the hysteresis of particle phase transitions, *J. Geophys. Res. Atmos.*, 113(D11),
1425 n/a-n/a, doi:10.1029/2007JD009368, 2008a.

1426 Wang, M., Gu, J., Yang, R., Zeng, L. and Wang, S.: Comparison of cloud type and
1427 frequency over China from surface, FY-2E, and CloudSat observations, vol. 9259, pp.
1428 925913–925914. [online] Available from: <http://dx.doi.org/10.1117/12.2069110>,
1429 2014.

1430 Wang, P. and Stammes, P.: Evaluation of SCIAMACHY Oxygen A band cloud
1431 heights using Cloudnet measurements, *Atmos. Meas. Tech.*, 7(5), 1331–1350,
1432 doi:10.5194/amt-7-1331-2014, 2014.

1433 Wang, P., Stammes, P., van der A, R., Pinardi, G. and van Roozendaal, M.:
1434 FRESCO+: an improved O₂ A-band cloud retrieval algorithm for tropospheric trace
1435 gas retrievals, *Atmos. Chem. Phys.*, 8(21), 6565–6576, doi:10.5194/acp-8-6565-2008,
1436 2008b.

删除的内容: <sub>

删除的内容: <sub>

删除的内容: <sub>

删除的内容: <sub>

删除的内容: <sub>

删除的内容: <sub>

1443 Wang, X., Huang, J., Zhang, R., Chen, B. and Bi, J.: Surface measurements of aerosol
1444 properties over northwest China during ARM China 2008 deployment, *J. Geophys.*
1445 *Res. Atmos.*, 115(D7), n/a-n/a, doi:10.1029/2009JD013467, 2010.

1446 Wang, Y., Penning de Vries, M., Xie, P. H., Beirle, S., Dörner, S., Remmers, J., Li, A.
1447 and Wagner, T.: Cloud and aerosol classification for 2.5 years of MAX-DOAS
1448 observations in Wuxi (China) and comparison to independent data sets, *Atmos. Meas.*
1449 *Tech.*, 8(12), 5133–5156, doi:10.5194/amt-8-5133-2015, 2015.

1450 Wang, Y., Lampel, J., Xie, P., Beirle, S., Li, A., Wu, D. and Wagner, T.:
1451 Ground-based MAX-DOAS observations of tropospheric aerosols, NO₂, SO₂ and
1452 HCHO in Wuxi, China, from 2011 to 2014, *Atmos. Chem. Phys.*, 17(3), 2189–2215,
1453 doi:10.5194/acp-17-2189-2017, 2017a.

1454 Wang, Y., Beirle, S., Lampel, J., Koukouli, M., De Smedt, I., Theys, N., Li, A., Wu,
1455 D., Xie, P., Liu, C., Van Roozendael, M., Stavrou, T., Müller, J.-F. and Wagner, T.:
1456 Validation of OMI, GOME-2A and GOME-2B tropospheric NO₂, SO₂ and HCHO
1457 products using MAX-DOAS observations from 2011 to 2014 in Wuxi, China:
1458 investigation of the effects of priori profiles and aerosols on the satellite products,
1459 *Atmos. Chem. Phys.*, 17(8), 5007–5033, doi:10.5194/acp-17-5007-2017, 2017b.

1460 Winker, D. M., Pelon, J., Coakley, J. A., Ackerman, S. A., Charlson, R. J., Colarco, P.
1461 R., Flamant, P., Fu, Q., Hoff, R. M., Kittaka, C., Kubar, T. L., Le Treut, H.,
1462 McCormick, M. P., Mégie, G., Poole, L., Powell, K., Trepte, C., Vaughan, M. A. and
1463 Wielicki, B. A.: The CALIPSO Mission, *Bull. Am. Meteorol. Soc.*, 91(9), 1211–1230,
1464 doi:10.1175/2010BAMS3009.1, 2010.

1465 Winker, D. M., Tackett, J. L., Getzewich, B. J., Liu, Z., Vaughan, M. A. and Rogers,
1466 R. R.: The global 3-D distribution of tropospheric aerosols as characterized by

删除的内容: <sub>

删除的内容: <sub>

删除的内容: <sub>

删除的内容: <sub>

1471 CALIOP, *Atmos. Chem. Phys.*, 13(6), 3345–3361, doi:10.5194/acp-13-3345-2013,
1472 2013.

1473 Zara, M., Boersma, K. F., De Smedt, I., Richter, A., Peters, E., Van Geffen, J. H. G.
1474 M., Beirle, S., Wagner, T., Van Roozendael, M., Marchenko, S., Lamsal, L. N. and
1475 Eskes, H. J.: Improved slant column density retrieval of nitrogen dioxide and
1476 formaldehyde for OMI and GOME-2A from QA4ECV: intercomparison, uncertainty
1477 characterization, and trends, *Atmos. Meas. Tech. Discuss.*, 1–47,
1478 doi:10.5194/amt-2017-453, 2018.

1479 Zhang, Q., Streets, D. G., Carmichael, G. R., He, K. B., Huo, H., Kannari, A.,
1480 Klimont, Z., Park, I. S., Reddy, S., Fu, J. S., Chen, D., Duan, L., Lei, Y., Wang, L. T.
1481 and Yao, Z. L.: Asian emissions in 2006 for the NASA INTEX-B mission, *Atmos.*
1482 *Chem. Phys.*, 9(14), 5131–5153, doi:10.5194/acp-9-5131-2009, 2009.

1483 Zhao, C. and Wang, Y.: Assimilated inversion of NO_x emissions over east Asia using
1484 OMI NO₂ column measurements, *Geophys. Res. Lett.*, 36(6), L06805,
1485 doi:10.1029/2008GL037123, 2009.

删除的内容:

1486 Zhao, H. Y., Zhang, Q., Guan, D. B., Davis, S. J., Liu, Z., Huo, H., Lin, J. T., Liu, W.
1487 D. and He, K. B.: Assessment of China's virtual air pollution transport embodied in
1488 trade by using a consumption-based emission inventory, *Atmos. Chem. Phys.*, 15(10),
1489 5443–5456, doi:10.5194/acp-15-5443-2015, 2015.

1490 Zhou, Y., Brunner, D., Spurr, R. J. D., Boersma, K. F., Sneep, M., Popp, C. and
1491 Buchmann, B.: Accounting for surface reflectance anisotropy in satellite retrievals of
1492 tropospheric NO₂, *Atmos. Meas. Tech.*, 3(5), 1185–1203,
1493 doi:10.5194/amt-3-1185-2010, 2010.

删除的内容: <sub>

删除的内容: </sub>

1497 Zhu, W., Xu, C., Qian, X. and Wei, H.: Statistical analysis of the spatial-temporal
1498 distribution of aerosol extinction retrieved by micro-pulse lidar in Kashgar, China,
1499 *Opt. Express*, 21(3), 2531–2537, doi:10.1364/OE.21.002531, 2013.

1500 Hendrick, F., Muller, J. F., Clemer, K., Wang, P., De Maziere, M., Fayt, C., Gielen,
1501 C., Hermans, C., Ma, J. Z., Pinardi, G., Stavrakou, T., Vlemmix, T., and Van
1502 Roozendael, M.: Four years of ground-based MAX-DOAS observations of HONO
1503 and NO₂ in the Beijing area, *Atmospheric Chemistry and Physics*, 14, 765-781,
1504 10.5194/acp-14-765-2014, 2014.

1505 Jethva, H., Torres, O., and Ahn, C.: A ten-year global record of absorbing aerosols
1506 above clouds from OMI's near-UV observations, in: *Remote Sensing of the*
1507 *Atmosphere, Clouds, and Precipitation VI*, edited by: Im, E., Kumar, R., and Yang, S.,
1508 *Proceedings of SPIE*, 2016.

1509 Schenkeveld, V. M. E., Jaross, G., Marchenko, S., Haffner, D., Kleipool, Q. L.,
1510 Rozemeijer, N. C., Veefkind, J. P., and Levelt, P. F.: In-flight performance of the
1511 Ozone Monitoring Instrument, *Atmospheric Measurement Techniques*, 10, 1957-1986,
1512 10.5194/amt-10-1957-2017, 2017.

1513 van Donkelaar, A., Martin, R. V., Spurr, R. J. D., Drury, E., Remer, L. A., Levy, R. C.,
1514 and Wang, J.: Optimal estimation for global ground-level fine particulate matter
1515 concentrations, *Journal of Geophysical Research-Atmospheres*, 118, 5621-5636,
1516 10.1002/jgrd.50479, 2013.

1517

删除的内容: Wang, Y., Lampel, J., Xie, P., Beirle, S., Li, A., Wu, D.,
and Wagner, T.: Ground-based MAX-DOAS observations of
tropospheric aerosols, NO₂, SO₂ and HCHO in Wuxi, China, from
2011 to 2014, *Atmospheric Chemistry and Physics*, 17, 2189-2215,
10.5194/acp-17-2189-2017, 2017.

We apply a number of criteria to ensure data quality of each pixel, mainly following Winker et al. (2013) and Amiridis et al. (2015). More detailed information about criteria to select the Level-2 are referred to Appendix A.

After the pixel-based screening, we aggregate the CALIOP data at the model grid (0.667° long. x 0.5° lat.) and vertical resolution (47 layers, with 36 layers or so in the troposphere). For each grid cell, we choose the CALIOP pixels within 1.5° of the grid cell center. The way to compile gridded CALIOP climatology aerosol extinction profiles is referred to Appendix B. CALIOP Level-2 data are always presented at the fixed 399 altitudes above sea level. To account for the difference in surface elevation between a CALIOP pixel and the respective model grid cell, we convert the altitude of the pixel to a height above the ground, by using the surface elevation data provided in CALIOP. We then average horizontally and vertically the profiles of all pixels within one model grid cell and layer. We do the regridding day-by-day for all grid cells to ensure that GEOS-Chem and CALIOP extinction profiles are coincident spatially and temporally. Finally, we compile a monthly climatological dataset by averaging over 2007–2015.

As discussed above, we choose the CALIOP pixels within 1.5° of a grid cell center. We test this choice by examining the aerosol layer height (ALH) produced for that grid cell. The ALH is defined as the extinction-weighted height of aerosols (see Eq. 1, where n denotes the number of tropospheric layers, ε_i the aerosol extinction at

layer i , and H_i the layer center height above the ground). We find that choosing pixels within 1.0° of a grid cell center leads to a noisier horizontal distribution of ALH, owing to the small footprint of CALIOP. On the other hand, choosing 2.0° leads to a too smooth spatial gradient of ALH with local characteristics of aerosol vertical distributions are largely lost. We thus decide that 1.5° is a good balance between noise and smoothness.

$$\text{ALH} = \frac{\sum_{i=1}^{i=n} \epsilon_i H_i}{\sum_{i=1}^{i=n} \epsilon_i} \quad (1)$$

Certain grid cells do not contain sufficient valid observations for some months of the climatological dataset. We fill in missing monthly values of a grid cell using valid data in the surrounding $5 \times 5 = 25$ grid cells (within ~ 100 km). If the 25 grid cells do not have enough valid data (see Appedix B for details next paragraph for details), we use those in the surrounding $7 \times 7 = 49$ grid cells (within ~ 150 km). A similar procedure is used by Lin et al. (2014b, 2015) to fill in missing values in the gridded MODIS AOD dataset.

3.2 Comparison to NASA CALIOP monthly climatology

We compare our gridded climatological profiles to NASA CALIOP Version 3 Level-3 all-sky monthly profiles at 532 nm (Winker et al. 2013). The NASA Level-3 data has a horizontal resolution of 2° lat. \times 5° lon. and a vertical resolution of 60 m (from -0.5 to 12 km above sea level). We combine NASA monthly data over 2007–2015 to construct a monthly climatology for comparison with our own compilation. We only choose aerosol extinction data in the troposphere with error less than 0.15 (the valid range given in the CALIOP dataset). If the number of valid monthly profiles in a grid cell is less than five (i.e., for the same month in five out of the nine years), then we exclude data in that grid cell; see the dark gray grid cells in Fig. 23c.

Several methodological differences exist between generating our and NASA CALIOP datasets. First, the two datasets have different horizontal resolutions. Also, we sample all valid CALIOP pixels within 1.5° of a grid cell center, whereas the NASA dataset samples all valid pixels within a grid cell. Besides, our CALIOP dataset involves several steps of horizontal interpolation, for purposes of subsequent cloud and NO_2 retrievals, which is not done in the NASA dataset. In addition, we match CALIOP data vertically to the GEOS-Chem vertical resolution, whereas the NASA dataset maintains the original resolution.

Figure 23c shows the spatial distribution of ALH in all seasons based on NASA CALIOP Level-3 all-sky monthly climatology. The horizontal resolution of NASA data is much coarser than ours; and NASA data are largely missing over the southwest with complex terrains. We choose to focus on the comparison over East China (the black box in Fig. 12a). Over East China, the two climatology datasets generally exhibit similar spatial patterns of ALH in all seasons (Fig. 23a, c). The NASA dataset suggests higher ALHs than ours over Eastern China, especially in summer, due mainly to differences in the sampling and regridding processes. Figure 34c further compares the monthly variation of ALH between our (black line with error bars) and NASA (blue filled triangles) datasets averaged over East China. The two datasets are consistent in almost all months, indicating that their regional differences are largely smoothed out by spatial averaging.

is aim at making rapid judgments on validity and trustworthiness of Earth Observation data and the derived climate data sets. It

第 25 页: [7] 删除的内容

Folkert Boersma

2018/6/28 AM10:51:00

essentially an ensemble data sets of satellite products provide

第 25 页: [8] 删除的内容

Jintai Lin

2018/6/21 PM5:46:00

, with a fully traceable quality assurance on all aspects of the NO₂, HCHO and carbon monoxide (CO) (Zara et al., 2018)